

An-Najah National University
Faculty of Graduate Studies.

**Complexes Design, Spectral, Structural and Biological
Activities of Novel Dicationic [Copper(II)/1,10-
phenanthroline/N-tridentate] 2bromide**

By
Muheeb Rafi Mohammad Fuqha

Supervisor
Prof . Ismail Warad

**This Thesis is Submitted in Partial Fulfillment of the Requirements for
the Degree of Master of Chemistry, Faculty of Graduate Studies, An-
Najah National University, Nablus, Palestine.**

2015

III
Dedication

I dedicate my thesis :

To my beloved parents and the family, for their prayers for me.

To my dear brothers and sisters .

To all of my friends.

To My doctors at the

An-Najah National University-Nablus.

and

Arab American University-Jenin.

Hashemite University-Jordan

To all People and Muslims in the world.

Acknowledgements

First of all, I thank Allah for giving me the strength and the patience that I needed to stay on the path of learning and finish my thesis.

The recognition of this work was only possible due to several people's collaboration, to which I desire to express my gratefulness.

I wish to thank my supervisor who were more than generous with their expertise and precious time. Special thanks to Prof Dr. Ismail Warad for his countless hours of reflecting, reading, encouraging, and most of all patience throughout the entire process.

My deep gratitude and thanks to the Faculty members of Science Department at An-Najah National University for granting me the opportunity to use their labs and equipments to pursue my thesis. Special thanks to lab technician Mr. Nafez Dwikkat for his guidance and ease my work in the Laboratory.

A special thank and gratitude for Biodiversity and Environmental Research Center, BEREC, Till, Nablus, Palestine and Jordanian people in the Hashemite university.

V
الاقرار

أنا الموقع ادناه مقدم الرسالة التي تحمل العنوان:

**Complexes Design, Spectral, Structural and Biological Activities of
Novel dicationic [Copper (II)/1,10-phenanthroline/N-tridentate]
2bromide.**

أقر بأن ما اشتملت عليه هذه الرسالة إنما هو نتاج جهدي الخاص، باستثناء ما تمت الإشارة إليه
حيثما ورد، وان هذه الرسالة ككل أو أي جزء منها لم يقدم من قبل لنيل أي درجة علمية أو بحث
علمي أو بحثي لدى أية مؤسسة تعليمية أو بحثية .

Declaration

The work provided in this thesis, unless otherwise referenced, is the
researcher's own work, and has not been submitted elsewhere for any other
degree or qualification.

Student Name:

اسم الطالب: مهيب رافع محمد قنعا

Signature:

التوقيع: مهيب رافع محمد قنعا

Date:

التاريخ: 2015/10/18

VI
List of Contents.

No.	Content	page
	Dedication	III
	Acknowledgments	IV
	Declaration	V
	List of contents	VI
	List of tables	VIII
	List of figures	IX
	List of images and schemes	XI
	Abstract	XII
	Chapter One: Introduction.	1
1.1	General background.	2
1.2	Organometallic chemistry.	2
1.3	Transition metal ions M ⁿ⁺ complexes.	3
	Chapter Two: Materials and methodology.	11
Part 1	Material and methods of [Cu(1,10-phen)(dien)]Br₂(1) and [Cu(1,10-phen)(dipn)]Br₂(2) Complexes.	12
1	Chemicals.	12
2	General procedure to synthesis complex 1 and 2.	12
2.1	[Cu(phen)(dien)]Br ₂ (1).	13
2.2	[Cu(phen)(dipn)]Br ₂ (2).	14
3	Physical Measurements.	14
4	Computational Details.	15
5	Single-Crystal X-Ray Data collection.	15
6	Biological studies.	17
6.1	Antioxidant activity.	17
6.2	Antimicrobial activity.	17
6.3	Antifungal Activity.	19
6.4	Cytotoxicity Determination.	20
6.5	DNA Binding Experiment.	21
Part 2	Material and methods of [Cu(2,2'-dpa)₂Cl]Cl (3) and [Cu(2,2'-dpa)(dien)]Cl₂(4) Complexes.	22
1	Materials and chemicals.	22
2	General procedure to synthesis complex 3 and 4.	22
2.1	[Cu(dpa) ₂ Cl]Cl (3).	22
2.2	[Cu(dpa)(dien)]Cl ₂ (4).	23
3	Physical Measurements.	24
4	Single-Crystal X-Ray Data collection.	24
	Chapter Three: Results and discussion.	26

VII

Part1	Synthesis, Spectral and Structural of [Cu(1,10-phen)(dien)]Br₂(1)and[Cu(1,10-phen)(dipn)]Br₂(2)Complexes.	27
1	Introduction.	27
2	Synthesis of complexes 1 and 2 .	28
3	IR Spectral Data.	29
4	Thermal analyses (TGA/DTA).	30
5	Crystal structure for complex 1 .	32
6	UV-Visible and ultraviolet spectra.	38
Part 2	Synthesis, Spectral and Structural of [Cu(2,2'-dpa)₂Cl]Cl(3)and[Cu(2,2'-dpa)(dien)]Cl₂(4) Complexes.	43
1	Introduction.	43
2	Synthesis of complexes 3 and 4 .	43
3	IR Spectral Data.	44
4	TGA/DTA Mass spectroscopy.	46
4.1	Thermal analysis (TGA/DTA).	46
4.2	TOF-Mass spectra.	48
5	UV-visible and ultraviolet spectra.	49
6	Crystal structure for complex 3 .	53
7	Hirschfield surface analysis of complex 3 .	56
Part 3	Biological Studies and activity of complex 1 and 2.	59
1	Antioxidant activity (β-Carotene assay).	59
2	Antibacterial and anti-Candida activity.	60
3	Antifungal Activity.	61
4	Cytotoxicity determination of compounds on HCT116 Cells.	62
5	DNA binding properties of complex 1 .	63
	Chapter four: Conclusion.	67
	Conclusion.	68
	References.	70
	الملخص	ب

VIII
List of Tables

Table No.	Title	Page
Table 1	Crystallographic Data and Structure Refinement Parameters for complex 1 .	16
Table 2	Crystallographic Data and Structure Refinement Parameters of complex 3 .	25
Table 3	Experimental X-Ray and calculated bond length of complex 1 by Time Dependent-Functional Theory.	32
Table 4	Major Bond angle (N-Cu-N) for complex 1 .	32
Table 5	Hydrogen bonds distances (Å) and angles (°).	37
Table 6	DFT energies and composition of selected highest occupied (H) and lowest unoccupied (L) molecular orbitals of complex 1 expressed in terms of composing fragments for complex.	41
Table 7	Computed excitation energies λ (nm), electronic transition configurations and oscillator strengths (f) for the optical transitions in the visible region of complex 1 transitions with $f \geq 0.004$ are listed .	42
Table 8	Calculated absorption wavelength, oscillator strength and molecular orbital contributions of UV-Vis electronic transitions, transitions with oscillator strength less than 0.02 are not listed.	51
Table 9	Calculated energies of the involved molecular orbitals in the electronic transitions and the percent distribution of these orbitals on Cu center, chloride ligand and organic ligand.	52
Table 10	measured bond length (Å) for Complex 3 crystal .	54
Table 11	Bond angle (N-Cu-N) for complex 3 crystal.	54
Table 12	Inhibition zone in (mm), each sample was done in triplicate.	61

List of Figures

No.	Title	Page
Figure 1	IR-KBr spectra of starting materials a)[CuBr ₂ (1,10-phen)], and b)[Cu(1,10-phen)(dien)]Br ₂ (1).	29
Figure 2	Thermo-gravimetric (TG/DTA) analysis of Cu(1,10-phen)(dipn)Br ₂ (2).	31
Figure 3	The ORTEP generated diagram of complex 1 with displacement ellipsoids drawn at 50% probability level.	33
Figure 4	Chain structure of complex 1 .	34
Figure 5	The layer structure of the complex 1 .	35
Figure 6	Chain structure of complex 1 and crystal packing.	35
Figure 7	Illustration of the N (π)...N interactions. View is perpendicular to the plane of the aromatic systems. All atoms are represented as wireframes except nitrogen atoms that are involved in the interactions as spheres.	36
Figure 8	UV-Visible spectra of complex 1 in water at room temperature (RT).	38
Figure 9	UV-Visible spectra of (a) CuBr ₂ (1,10-phen) addition (b) [Cu(1,10-phen)(dipn)]Br ₂ (2), dissolved in water at room temperature (RT).	39
Figure 10	Isodensity plots of some selected MOs (α-spin and β-spin) of complex 1 .	40
Figure 11	FT-IR spectra of complex 3 , and complex 4 of copper(II) chloride.	45
Figure 12	TG/DTG Thermal curves of the (a) complex 3 , and (b) complex 4 .	47
Figure 13	FT-IR spectra of (Cu=O) residues.	48
Figure 14	TOF-MS spectra of complex 3 [Cu(dpa) ₂ Cl]Cl and complex 4 [Cu(dpa)(dien)]Cl ₂ .	49
Figure 15	UV-Visible spectra of [Cu Cl (2,2'-dpa) ₂]Cl (3) and [Cu(2,2'-dpa)(dien)]Cl ₂ (4) dissolved in water at RT.	50
Figure 16	The Calculated UV-Vis spectrum of complex 3 in water.	50
Figure 17	β-LUMO molecular orbital of complex 3 .	51
Figure 18	UV- spectra of [Cu Cl (2,2'-dpa) ₂]Cl green spectra and [Cu(2,2'-dpa)(dien)]Cl ₂ blue spectra dissolved in water at (RT).	53
Figure 19	The ORTEP generated diagram of complex 3 with	55

	displacement ellipsoids drawn at 30% probability level, Hydrogen atoms are omitted for clarity.	
Figure 20	The crystal structure and packing of the complex 3 .	55
Figure 21	Chain structure of the complex 3 .	56
Figure 22	Hirschfield surfaces comprising dnorm surface plots for complex 3 .	57
Figure 23	Fingerprint plots of the complex 3 molecule.	58
Figure 24	Changes in values of absorbance with time for starting compounds and products, BHA and Gallic acid as assessed by β -carotene-linoleic acid assay over 120 min.	59
Figure 25	Antioxidant activities of methanol solution of the three copper compounds, and BHA and Gallic acid as assessed by β -carotene linoleic acid assay over 120 min.	60
Figure 26	Anti-dermatophytes activity of $\text{CuBr}_2(\text{phen})$, 1 and 2 complexes (%inhibition) at 300 $\mu\text{g/mL}$.	62
Figure 27	MTT assay in HCT-116 colon cancer cells after an overnight treatment with various concentrations of the complexes 1 and 2 .	63
Figure 28	Electronic spectral titration of complex 1 with CT-DNA at 620nm in Tris-HCl buffer; [complex]= 5×10^{-3} ; [DNA]: a= 0.0, b= 1.0×10^{-4} , c = 4.0×10^{-4} , d= 8.0×10^{-4} , e = 1.0×10^{-3} , f = 3.0×10^{-3} , h = 6.0×10^{-3} , i = 1.0×10^{-2} , j= 2.0×10^{-2} , k = 4.0×10^{-2} M.	64
Figure 29	Absorption plot against [DNA] to confirm the exponential decreasing relation at $\lambda = 620$ nm.	64
Figure 30	Plot of $[\text{DNA}]/(\epsilon a - \epsilon f)$ versus [DNA] for the absorption titration of DNA with the complex 1 .	65

List of Images and Schemes

No.	Title	Page
Image 1	Magnesium in chlorophyll pigments, and Iron in hemoglobin blood.	3
Image 2	Collected crystal by microscope for Cu(1,10phen)(dien)Br ₂ (1).	13
Image 3	Chemical products of copper(II)bromide (1) and (2) complexes.	13
Scheme 1	Syntheses of [Cu(1,10-phen)(dien)]Br ₂ (1) and [Cu(1,10-phen)(dipn)]Br ₂ (2) complexes.	28
Scheme 2	Synthesis [Cu(2,2'-dpa) ₂ Cl]Cl (3) and [Cu(2,2'-dpa)(dien)]Cl ₂ (4) complexes.	44

**Complexes Design, Spectral, Structural and Biological Activities of
Novel Dicationic [Copper(II)/1,10-phenanthroline/N-tridentate]
2bromide.**

By

Muheeb Rafi Mohammad Fuqha

Supervisor

Prof . Ismail Warad

Abstract

Four novel new monocationic and dicationic mixed copper(II) complexes, of general formula $[\text{Cu}(1,10\text{-phen})(\text{dien})]\text{Br}_2$ (**1**), $[\text{Cu}(1,10\text{-phen})(\text{dipn})]\text{Br}_2$ (**2**), $[\text{Cu}(2,2'\text{-dpa})_2\text{Cl}]\text{Cl}$ (**3**) and $[\text{Cu}(2,2'\text{-dpa})(\text{dien})]\text{Cl}_2$ (**4**) [phen=phenanthroline, dien=Diethylenetriamine, dipn=Diproplenetriamine, and dpa=Dipyridylamine], synthesized in very good yields. These complexes were characterized by spectroscopic, elemental analysis, UV-visible, IR-Spectroscopy, thermal analysis TGA/DTA and X-ray crystallographic techniques. Single crystal X-ray diffraction data for complex **1** showed a distorted square pyramidal geometry around Cu(II) ion with three solvated water molecules and complex **3** the same distorted square pyramidal geometry around Cu(II) ion.

Biological studies of Antioxidant, Antimicrobials, Antifungal assays and Cytotoxicity and CT-DNA binding were conducted to evaluate the biological activities of complex **1**, **2**. These complexes exhibit a promising antimicrobial effect against an array of microbes at 200 $\mu\text{g}/\text{mL}$ concentration. The antiproliferative assay shows a high potential of these complexes to target Human keratinocyte cell line with IC_{50} values of 155 and 152 μM .

XIII

The CT-DNA binding of complex **1** was evaluated using electronic absorption spectroscopy at $\lambda_{\text{max}} = 620\text{nm}$, such complexes showed high DNA binding, the value of binding constant ($K_b = 8.6 \times 10^4 \text{ M}^{-1}$) which is in a very good range. The biological activities of complex **1** and complex **2** have shown new chemotherapy, antimicrobial, high DNA binding, and high anticancer activities.

The theoretical absorption spectra of complex **1** and **3** in water were modeled by time-dependent density functional theory (TD-DFT) using Gaussian program.

Chapter One

Introduction

Chapter One

Introduction

1.1 General Background.

Medicinal organometallic chemistry comprises the major of a metal ion into a biological body system either by fortuity or by intention, the intentional starting of metal ions into a biological system will be either for chemo-therapeutic or diagnostic works, characters of metal ions that they are easily oxidized to lose electrons from the elemental or metallic state to form positively charged ions which tend to be more reactive and soluble chemical reagents, This cationic form for metal ions plays their rule in biochemistry. Whereas, metals are electron deficient, most biological molecules such as proteins and DNA are electron rich. The attraction of these opposing charges leads to a general tendency for metal ions to bind and to interact with biological molecules [1].

1.2 Organometallic chemistry.

Organometallic chemistry is important in chemical and biological applications, Many living organisms that contain complexes building from metal bonded with bulk organic group ligand by covalent and coordinating bond, for example hemoglobin in human and animals blood constructed from Fe^{2+} ions that are connected with bulky groups with nitrogen donor ligand, and chlorophyll in plants constructed from Magnesium metal ions Mg^{2+} and imine ligand [2, 3].

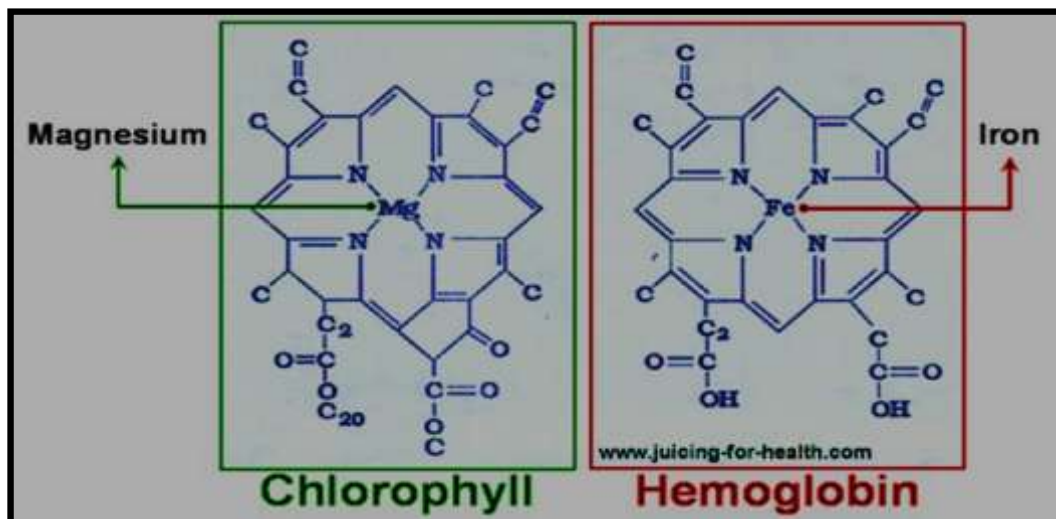


Image 1: Magnesium in chlorophyll pigments ,and Iron in hemoglobin blood.

The chemistry of transition metal ion complexes has received considerable attention, due to their catalytic and bioinorganic relevance, these complexes are important in pharmaceutical area, due to their potential biological activities like as antibacterial, antiviral, antifungal ,antimalarial and antitumor [4, 5]. Organometallic chemistry complexes that are used in a wide area as catalysis in synthesis of organic compounds, for example: Grignard reagent $[RMX]$ is an important methodology for conversion aldehydes and ketones to alcohols. Grignard reagents $[RMX]$ that are excellent for preparation of optically active stereochemically molecules. that are very important in medicine as drugs. The organometallic compound synthesis have provide many chemicals reagent that are used as additives material and plasticizers [3, 4].

1.3 Transition metal ions M^{n+} complexes.

Transition metal ions can coordinate a ligand in a precise three-dimensional configuration thus allowing the tailoring of the molecule to recognize and interact with a defined molecular target. This is further

enhanced by the diversity of chemical modification of ligands and selection of metal ions to form more stabilized complex [4, 5].

Metal ions possess different oxidation states which not only allows for modification of the three-dimensional space into which the molecule can fit, but significantly permits them to participate in biological oxidation-reduction chemistry and determining the coordination number [6-8].

In addition, the ability to undergo ligand exchange reactions offers unique opportunities for metal ions to interact and coordinate with biologically important ions and molecules. Medicinal inorganic chemistry is comparatively a new discipline, which developed after the serendipitous discovery of the anti-tumor activity of cis-platin [9]. The clinical success of this platinum complex has stimulated considerable interest in the search for new metal complexes as modern therapeutics, diagnostic and radiopharmaceutical agents [10].

In this direction, copper and zinc complexes are used in the treatment of many diseases including cancer cells [10-12]. Cobalt complexes have been investigated as potential hypoxia-activated pro-drugs. Meanwhile, chromium Cr^{n+} , manganese Mn^{n+} and iron Fe^{n+} complexes ions have been used for antibacterial activity. Zinc ions Zn^{n+} is an essential for the structure regulation and catalytic action of over 300-400 enzymes [13, 14]. It is a well-known fact that the biological properties of metals are determined both by speciation and the ligand present around the metal center. As an example, the simple chloride salt of platinum, such as (PtCl_4) are known as sensitizers eliciting a potential fatal allergic reaction, whereas

the neutral complex cis-dichlorodiamine platinum(II) complex, $[\text{Pt}(\text{NH}_3)_2\text{Cl}_2]$, is one of the most successful cancer drugs of recent years [15, 16].

One of the potential approaches in anticancer chemistry is focused on the design of new metal compounds with different substituents and labile sites which may increase their cytotoxicity specifically to cancer cells. The wide range of coordination numbers and geometries, accessible redox states, thermodynamic and kinetic characteristics and the intrinsic properties of the cationic metal ion and ligand itself offer the medicinal chemist a wide spectrum of activities that can be exploited [14-16].

Copper, being as a trace element, is present in parts per million concentration (ppm) range in biological bodies systems. The element functions as a key cofactor in a diverse array of biological oxidation reduction reactions [2]. copper that is containing proteins (hemocyanin, tyrosinase, chatecol oxidase) are involved in various processes in living systems [3-6]. copper ions $\text{Cu}(\text{II})$ is known to form complexes with a variety of molecular geometries and in these complexes, the configuration makes the distorted structure in octahedral and tetrahedral and square pyramidal, trigonal bipyramidal symmetries.

The distortion is usually seen as axial elongation, consistent with the lability and geometric flexibility of the complex, typical $\text{Cu}(\text{II})$ complexes have square planar or square pyramidal geometries with weakly associated ligands in the axial position. Trigonal bipyramidal coordination's are also known for $\text{Cu}(\text{II})$ complexes. In some cases, bridged complexes in which

two or more Cu(II) ions are linked by oxygen or nitrogen donor or other anionic ligands [7, 8].

The design and synthesis of 1,10-phenanthroline and their derivatives metal complexes are fascinating areas of research due to their important and promising applications in chemistry, physics, material and biological sciences [1, 2].

In spite of a large number of antibiotics and chemotherapeutics available for medical use, at the same time the emergence of old and new antibiotic resistance created in the last decades revealed a substantial medical need for new classes of antimicrobial agents [20].

There is a real perceived need for the discovery of new compounds endowed with antimicrobial activity, possibly acting through mechanism of action, which is distinct from those of well-known classes of antimicrobial agents to which many clinically relevant pathogens are now resistant [21].

Some metals have been used as drugs and diagnostic agents to treat a variety of diseases and conditions. Platinum compounds, cis-platin ($\text{cis-Pt}(\text{NH}_3)_2\text{Cl}_2$), carboplatin and oxaliplatin are among the most widely used cancer therapeutic agents. Gold drug (myocrisin and auranofin) are used for the treatment of rheumatoid arthritis. Another important aspect of medicinal inorganic chemistry is the development of radiopharmaceuticals and diagnostic agents [22]. the use of lanthanides and transition metals like

(Gd, Fe, Cu, Mn) as paramagnetic contrast agents for magnetic resonance imaging is becoming more exciting with the development of new complexes having the ability to target specific tissues and physiological states [23].

The coordination chemistry of N₃-dipyridylamine ligand and its derivatives has now been the subject of a number of several studies, due to their coordination versatility and affinity for most of metal ions [1].

2,2'-Dipyridylamine (dpa) and 2,2'-bipyridine ligands are very similar in chelating behaviors. For such reasons they are employed in the synthesis of numerous mono and polynuclear metal complexes [2]. The mononuclear complex (dpa) behaves as a bidentate chelating ligand bonded through both the terminal pyridine nitrogen donor sites. However, it also interacts in an unusual monodentate binding mode, depending upon requirements around the metal center [3]. A number of polydentate ligands with dipyridylamine as the fragment of chelate ligand system have also been developed and employed in the studies ranging from supramolecular chemistry and metal coordination to synthesis of new luminescent materials [4, 5]. This peculiar property of (dpa) and its derivatives induces either electronically or stereochemically in the systems and have been observed in a number of metal complexes [6-9]. Furthermore, the amine proton of (dpa) becomes more acidic upon complexation to the metal center and both protonated as well as deprotonated (dpa) complexes based on a number of metal ions that have been studied [10-12]. Loss of this proton is believed to result in planar ligand configuration in the complexes[13]. Platinum(II) and

Palladium(II) complexes of both the (dpa) and extended derivatives have also been investigated as potential anticancer agents due to their structural similarity to cis-platin [14-16]. The chemistry reaction of pyridine, bipyridine (bipy), terpyridine (terpy), phenantroline (phen), naphthyridine (naphthy) and pyridine-pyridazine (pyridaz) have received more and more attention since the late 19th century [38-40]. Coordination chemistry of these ligands with different metals to ligand ratio results in different geometries, such as tetrahedral [41], square planer, pentagonal, bipyramidal [42], or octahedral [43, 44]. These organic ligands containing unsaturated nitrogen atoms can be regarded as soft Lewis bases [45]. Transition metal complexes containing tridentate nitrogen donor ligand like (dien) or (dipn) have been of interest for many years [1-5]. The determination of the structure of these complexes in solution is indispensable for the understanding of some biological processes [16, 17]. In general, copper(II) complexes have been found to have possible medical uses in the treatment of many diseases including cancer [12, 13]. It has been known that the anti-cancer activity of some copper(II) complexes may be based on their ability to inhibit DNA synthesis [12]. These complexes are expected to be more permeable through the cell membrane [14-18].

The chemistry of Cu(II), involving tridentate and didentate amines ligands, that attracted a considerable interest due to their chelating properties [1]. The molecular structure of five-coordinated copper(II) complexes revealed an extensive variability, ranging from regular trigonal

bipyramidal to regular square based pyramidal with most complexes displaying a structure that is intermediate between the two extremes. In such materials, interesting properties and potentials in spectroscopy, electrochemistry, biological activity and magnetism can be introduced from either the inorganic species or the organic linker molecule [2-6]. Metal complexes with tridentate amine ligands, such as diethylenetriamine (dien) have been thoroughly investigated [7-11]. Complexes containing the analogous dipropylenetriamine (dipn) ligand have not received much attention, interestingly no reports on the synthesis of copper(II) complexes containing the dipropylenetriamine.

In this research, the synthesis of new mono and dicationic of $\text{Cu}(\text{phen})(\text{dien})\text{Br}_2$ (**1**), $\text{Cu}(\text{phen})(\text{dipn})\text{Br}_2$ (**2**), $[\text{Cu}(\text{dpa})_2\text{Cl}]\text{Cl}$ (**3**) and $[\text{Cu}(\text{dpa})(\text{dien})]\text{Cl}_2$ (**4**) complexes have been reported from CuBr_2 , CuCl_2 , with using of ultrasonic wave and dipyridylamine, phenanthroline and the tridentate (dien) or (dipn) displaced the bromide or chloride in $\text{CuBr}_2(\text{phen})$ and $\text{CuCl}_2(\text{dpa})$ from internal coordination sphere to the outer sphere to form new stable dicationic water soluble complexes [**1**, **2** and **3**, **4**].

Such coordination was monitored proved by UV-visible and IR spectroscopy and confirmed by single crystal X-ray structure as complex **1** and complex **3**, Biological studies of the first two complexes **1** and **2** are also discussed and studied. The absorption spectrum of complex **1** in water was modeled by time-dependent density functional theory (TD-DFT) [13]. The discovery and development of antibiotics among the most powerful and successful achievement of modern science and technology for the

control of infectious diseases , However, the increasing resistance microbial to antibiotics in use nowadays necessitates the search for new compounds with potential effects against pathogenic bacteria. The chemical preparation and physical properties have been described by various worker For developing potential antibiotic metal complexes have drawn attention of many investigations [19].

The treatment of infectious diseases still remains an important and challenging problem because of combination of factors including emerging infectious diseases and the increasing number of many drug resistant microbial pathogens [19].

Metal ions and their complexes have large activity in biological applications because of their cationic properties, modularity, reactivity, redox chemistry, photochemical reactions, and precisely defined three dimensional structures. They have been investigated and used as anticancer chemical reagents [24], artificial nuclease [25-27], acceptors or donors in the DNA mediated electron, hole, energy transfer [28-32], and probes for nucleic acids structures [33-37]. The catalytic effects of the various metal ions complexes on DNA strand breakage through a hydrolytic or oxidative mechanism are well known [38].

Chapter Two
Materials and Methodology

Chapter Two

PART 1:Material and methods of [Cu(1,10-phen)(dien)]Br₂ (1)and [Cu(1,10-phen) (dipn)]Br₂ (2) Complexes.

1. Chemicals.

All the reagents 1,10-phenanthroline (phen), diethylenetriamine (dien) and dipropylenetriamine (dipn), CuBr₂ used were of analytical grade and purchased from Sigma-Aldrich and used as received .

2. General procedure to synthesis complex 1 and 2 .

In a beaker (0.45g , 2mmol) of CuBr₂(phen) was suspended in 20 mL of ethanol under ultrasound waves, 2mmol of diethylenetriamine or dipropylenetriamine were dissolved in 10 mL of water and then added drop wise to the previous solution.

The mixture was left under stirring and ultrasound waves for 10 min until the solution turn to deep blue. The solvents were then removed under vacuum and the remaining solid was washed with isopropanol, dichloromethane and then dried under vacuum. Crystals of complex **1** suitable for X-ray structural analysis as seen in image **2** have been obtained by slow evaporation of water solution from the complex as shown in Image **3**.

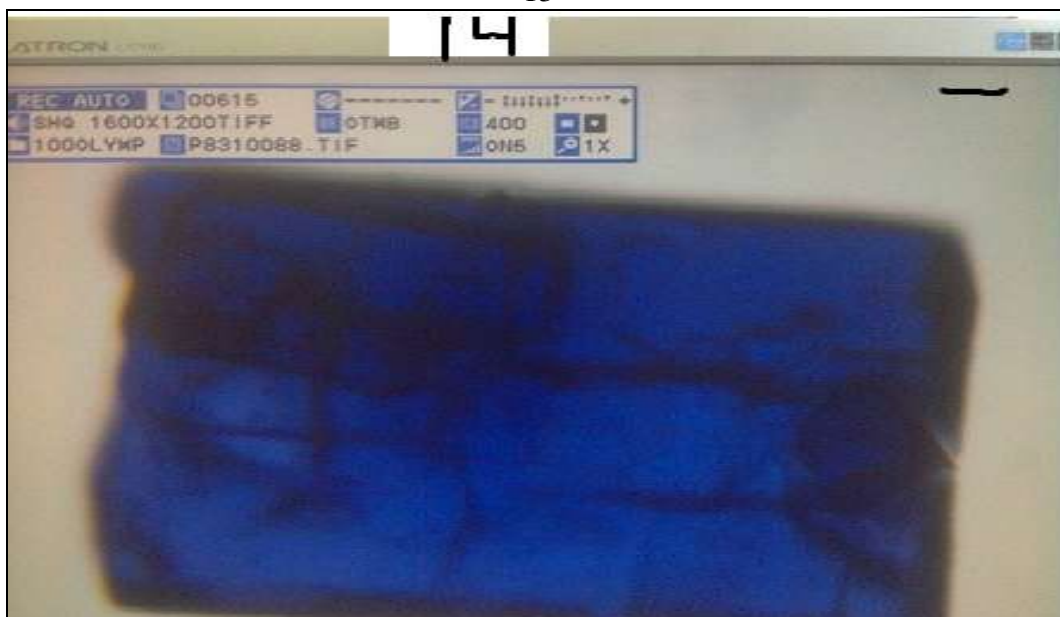


Image 2. Collected crystal by microscope for $\text{Cu}(\text{1,10phen})(\text{dien})\text{Br}_2$ (1).



Image 3. Chemical products of copper(II)bromide **1** and **2** complexes.

2.1 $[\text{Cu}(\text{phen})(\text{dien})]\text{Br}_2$ (1):

Yield (849.1mg) , and percentage yield = 84%, melting point (M.p) =180-184°C, MS m/z 505.2 $[\text{M}^+]$ for $\text{C}_{16}\text{H}_{21}\text{Br}_2\text{Cu N}_5$:

Calculated; C=37.92%, H=4.18%, N=13.82% .

Found; C=37.81%, H=4.10 %, N=14.62%.

IR (KBr, ν cm^{-1}): (ν H_2O) =3460, (ν H-N)=3380 and 3280, (ν C-H of phenyl)=3120, (ν C-H)=2930, (ν N-H)=1580, (ν N-C)=1160, (ν Cu-N)=620 and 540, UV-Visible spectra in water $\lambda_{\text{max}}(\epsilon_{\text{max}}/\text{M}^{-1}.\text{cm}^{-1})$:($1.6 \times 10^3 \text{M}^{-1}.\text{cm}^{-1}$) at 282nm, and($3.5 \times 10^2 \text{M}^{-1}.\text{cm}^{-1}$) at 620 nm.

2.2 [Cu(phen) (dipn)]Br₂ (2):

Yield (956.6mg),and percentage yield=89.5%,melting point (M.p)= 190-193°C, MS m/z 533.2 [M^+] for $\text{C}_{18}\text{H}_{25}\text{Br}_2\text{Cu N}_5$:

Calculated; C=40.43%, H=4.71%, N=13.10%.

Found; C=40.22%, H=4.64%, N=13.08%.

IR (KBr, ν cm^{-1}): (ν H_2O)=3440, (ν H-N)=3360 and 3270, (ν C-H of phenyl) =3160, (ν C-H)=2940, (ν N-H)=1560, (ν N-C)=1180, (ν Cu-N) 610 and 520, UV-Visible in water $\lambda_{\text{max}}(\epsilon_{\text{max}}/\text{M}^{-1}.\text{cm}^{-1})$:($1.6 \times 10^3 \text{M}^{-1}.\text{cm}^{-1}$) at 280 nm, ($3.0 \times 10^2 \text{M}^{-1}.\text{cm}^{-1}$) at 610nm.

3. Physical Measurements.

Microanalyses (C, H, N) were performed using an Elementar Varrio EL analyzer. The FT-IR spectra ($4000 - 200 \text{cm}^{-1}$) were obtained from KBr discs with a Perkin-Elmer 621 spectrophotometer.

Thermal analyses were carried out with TA instrument SDT- Q600 in air.

Electronic spectra were recorded in water at room temperature on Pharmacia LKB-Biochrom 4060 spectrophotometer.

FAB-MS data were obtained a Finnegan 711A (8 kV), modified by AMD and reported as mass/charge (M/z), respectively.

4. Computational Details.

Full geometry optimization of complex **1** was carried out using density functional theory (DFT) at the B3LYP level [57]. All calculations were carried out using the GAUSSIAN 09 program package with the aid of the Gauss View visualization program [58].

For C, H and N the cc-pvdz basis set were assigned, while for Cu and Br, the LanL2DZ basis set with effective core potential were employed [59]. Vertical electronic excitations based on B3LYP optimized geometries were computed using the time-dependent density functional theory (TD-DFT) formalism in water using polarizable continuum model (PCM) [60-63]. Gauss Sum was used to calculate the fractional contributions of various groups to each molecular orbital [64].

5. Single-Crystal X-Ray Data collection.

Crystals of complexes **1** was grown by a slow evaporation of water. A suitable block like elongated green crystals were mounted with Epoxy on a glass fiber and the diffraction data were collected at room temperature using an Oxford X caliber diffractometer (Mo K α radiation, $\lambda=0.7107$ Å). Data was reduced and processed to give *hkl* files using CrysAlisPro software [47]. The structures were solved by direct methods and refined by least-squares method on F² using the SHELXTL program package [48]. Carbon bound hydrogen atoms were placed in calculated positions and refined isotropically using a riding model, whereas, the six hydrogen atoms of the three water of solvation were located in a difference Fourier map and were refined isotropically. All non-hydrogen atoms were refined anisotropically.

Highest peak and deepest hole are 0.949 and - 0.503 e^{Å³}. Details of crystal data collection and refinement are given in Table 1.

Table 1. Crystallographic Data and Structure Refinement Parameters for complex 1.

Complex 1.	
Empirical formula	CuC ₂₈ H ₃₅ Br ₂ N ₇ O ₃ C ₁₆ H ₂₁ Br ₂ CuN ₅ .Phen.3H ₂ O
Formula weight	740.99 g/mole
Temperature	293(2) K
Wavelength	0.71073 Å
Crystal system	Monoclinic
Space group	P121/n1
Unit cell dimensions	a = 12.6411(13) Å, α = 90°. α = 95.1135(6)°. b = 19.422(3) Å, β = 111.016(12)°. c = 13.7128(13) Å, γ = 90°.
Volume	3142.7(6) Å ³
Z	4
Density (calculated)	1.566 Mg/m ³
Absorption coefficient	3.279 mm ⁻¹
F(000)	1500
Crystal size	0.4687 x 0.2661 x 0.2059 mm ³
Theta range for data collection	3.18 to 26.00°.
Index ranges	-15 ≤ h ≤ 15 -23 ≤ k ≤ 14 -15 ≤ l ≤ 16
Reflections collected	13451
Independent reflections	6161 [R(in t) = 0.0344]
Completeness to theta = 27.50°	99.8 %
Absorption correction	Analytical
Max. and min. transmission	0.652 and 0.395
Goodness-of-fit on F ²	1.012
Final R indices [I > 2sigma(I)]	R1 = 0.0602, wR2 = 0.1409
R indices (all data)	R1 = 0.1130, wR2 = 0.1614
Largest diff. peak and hole	0.949 and - 0.503 e ^{Å⁻³}

6. Biological studies.

6.1 Antioxidant activity:

β -carotene bleaching assay was conducted according to the method described by [49] with some modification. Briefly 1mL of a β -carotene solution (0.5mg / mL chloroform) was pipetted into a round bottom flask containing 20 μ L of linoleic acid and 250 μ L of Tween 20. After the removal of chloroform using rotary vacuum evaporator at 45 °C, 50mL of deionized water were added with vigorous agitation. One hundred eighty micro liters of the emulsion were added to 20 μ L of test compounds at varying concentrations in 96-well micro titer plate. The absorbance was measured at 470 nm immediately against a blank consisting of the emulsion without β -carotene and after 2h of incubation at 50°C using a spectrophotometer (Biotek USA). Degradation rate (dr) of the sample was calculated according to the first order kinetics as described by this equation: $dr \text{ of sample} = (\ln [A_0/A_t])/t$ [50].

where: ln = natural log; A_0 = initial absorbance at time 0 ; A_t = absorbance at 120 min of incubation; $t = 120$ min and $dr =$ degradation rate. Antioxidant activity (AA) was expressed as percent of inhibition relative to the control by using the equation:

$$AA\% = ([dr \text{ control} - dr \text{ sample}] / dr \text{ control}) \times 100\%.$$

6.2 Antimicrobial activity :

Microorganisms: The microorganisms used include: *Staphylococcus aureus* (ATCC 25923), *Escherichia coli* (ATCC 25922), *Klebsiella pneumonia*

(ATCC 13883), *Proteus vulgaris* (ATCC 13315), *Pseudomonas aeruginosa* (ATCC 27853), *Salmonella typhimurium* (ATCC14028), *Candida albicans* (CBS 6589, CBS 9120, and three other *Candida* strains isolated from different clinical specimens and identified using standard procedures: BERCN43A, BERCN72B, BERCN66C), and *Microsporium canis* (CBS132.88, BERC-EH-MC13), *Trichophyton rubrum* (BERC-EH-TR9). All microorganisms were provided from the collection held by the Biodiversity and Environmental Research Center, BERC.

Disk Diffusion Assay test:

The antimicrobial activity for the complexes ($\text{CuBr}_2(\text{phen})$, **1** , and **2**) was tested against six bacterial strains by the disk diffusion described by the Clinical and Laboratory Standards Institute (CLSI), M02-A11 document [51, 52].

The complexes were dissolved in methanol to a final concentration of 25mg/mL and sterilized by filtration through a 0.45 μm membrane filter. Antimicrobial tests were then carried out using an inoculum containing 10^6 bacterial cells or 10^8 yeast cells per 1mL to spread on Muller-Hinton agar plate. Compound impregnated discs with 25 μL of compound solution (1.25mg/disc) were placed on the inoculated agar and incubated at 37 $^\circ\text{C}$ for 24hours for bacteria and for 48hours for *C. albicans*. On each plate an appropriate reference antibiotic disc was applied depending on the test microorganisms [53].

Gentamicin served positive control for bacteria, whereas amphotericin-B served as a positive control for *C. albicans*. Reference antibiotic discs

containing 5mg antibiotic/disc were used. Minimal Inhibitory Concentration (MIC) was obtained according to the method described by [54], an adaptation of the standard method published by CLSI and the European Committee on Antimicrobial Susceptibility Testing (EUCAST) using the broth micro dilution procedure [55].

A working solution of 25mg/mL of each compound was prepared in sterile distilled water. The 96-well plate was prepared by adding 100 μ L of each compound to a final concentration of 5mg/mL to the first well. Then serial dilutions were made with MHB(Mueller-Hinton broth, Merck, Germany) in the other wells, to final volume of 100 μ L. At each well, 100 μ L of each bacterium was added (*S.aureus*, *E.coli*, *K.pneumonia*, *Pr.vulgaris*, *Ps.Aeruginosa*, *S. typhimurium*). The range of the complexes concentration was between 9 μ g/mL –1250 μ g/mL. Drug-free and bacteria controls were also included.

The plates were incubated for 24h at 37°C. The MIC value was determined by the observation of the concentration that did not show any growth, by contrast with the bacteria control. The procedure was made in triplicate for each compound and bacteria combination, in at least 3 independent assays.

6.3 Antifungal Activity:

All test isolates were inoculated onto SDA plates and incubated at 25°C for 7-10 days to obtain young, actively growing cultures consisting of mycelia and conidia. Antimycotic activity was carried out by the poisoned-food technique [56].

Different concentrations of each compound were incorporated in pre-sterilized SDA medium to prepare a series of concentrations (100, 200, 300 μ g/mL). The required amount of the compound or reference antimycotic was dissolved in 2mL sterile distilled water, sterilized by filtration through a 0.45-mm membrane filter, and then mixed with the amount of pre-sterilized SDA medium required in order to give the required concentration.

A mycelial disc, 5mm in diameter, cut from the periphery of the 7-10 day-old cultures, was aseptically inoculated onto the medium. In controls, sterile distilled water was used instead of compound. The inoculated plates were then incubated at 25°C and the colony diameter measured and recorded after 7days. The percentage of mycelial inhibition was calculated as follows: % Mycelial inhibition= $[(dc - dt)/dc] \times 100\%$.

dc = colony diameter in control, dt =colony diameter in treatment.

Three replicate plates were used for each treatment, in independent assays.

6.4 Cytotoxicity Determination:

The tetrazolium dye (MTT) is widely used to assess the viability of cells. The MTT mediated cytotoxicity and cytostatic assay, based upon the ability of living cells to reduce 3-[4,5-dimethylthiazol-2-yl]-2,5diphenyl tetrazolium bromide (MTT) into formazan by mitochondrial succinate dehydrogenase in viable cells. Colorectal carcinoma cell line (HCT-116) was purchased from the American Type Culture Collection (ATCC) and used in this study. Cells were maintained in myoblast monolayer culture,

grown under an atmosphere of 95% air and 5% CO₂ in RPMI 1640 supplemented with 10% fetal calf serum (FCS), 1mM L-glutamine, 100U/mL penicillin and 0.1mg/mL streptomycin. Cells with 70-80% confluence, were detached from the cultured flask by treatment with 0.05% trypsin- EDTA and a suspension of (2.0×10^4 cell/well) viable cells were seeded in a 96-well plate and incubated for 24h. Cells then were incubated with the complexes at concentrations up to 200 μ M.

After 24hour of incubation, 100 μ L of 3-(4,5-dimethylthiazol-2-yl)-2,5-diphenyl tetrazolium bromide (MTT, Sigma) solution (0.5mg/mL) were added to each well and incubated at 37°C for 4h. The medium was removed, and the formazan crystals were solubilized by acidified 100 μ L isopropanol (0.1N HCl). The absorbance of the MTT formazan was determined at 570nm in an Elisa reader. Cell viability was defined as the ratio (expressed as a percentage) of absorbance of the compound treated cells relative to untreated cells. The procedure was made in triplicate for each compound, at least, in 3 independent assays.

6.5 DNA Binding Experiment:

The (DNA) binding experiments were done in pH=7.4, Tris-HCl buffer with complex **1** dissolved in distilled water. The Calf-thymus (CT-DNA) concentration was determined by absorption spectroscopy using the molar absorption coefficient $350.4\text{M}^{-1}\text{cm}^{-1}$ at 620 nm.

Absorption spectral titration experiment was performed at constant complex **1** concentration 5×10^{-3} M and different CT- DNA concentration 0- 0.04M. After addition of DNA to complex **1**, the resulting solution was

allowed to equilibrate at 25°C for 10min, after which absorption spectra were noted.

PART 2:Material and methods of [Cu(2,2'-dpa)₂Cl]Cl (3) and [Cu(2,2'-dpa)(dien)]Cl₂ (4) Complexes.

1. Materials and chemicals.

All the reagents CuCl₂, and 2,2'-dipyridylamine and solvent: Methanol, ethanol, isopropyl alcohol, chloroform used were of analytical grade and purchased from Sigma-Aldrich and used as received.

2. General procedure to synthesis complex 3 and 4 .

2.1 [Cu(dpa)₂Cl]Cl (3):

In 10 mL of methanol (2mmol) of CuCl₂.4H₂O was suspended under ultrasound waves, aqueous solution (10mL) of equivalent of dpa (4mmol) was added drop wise to the solution under stirred and ultrasound waves atmosphere for 5min until the green precipitate was formed; the product complex was filtrated, then washed by n-hexane and dichloromethane, then dried under vacuum. Crystals suitable for X-ray structural analysis have been obtained by slow evaporation of water solution of the complex. The complex was isolated as green powder and Crystals were grown by a slow evaporation of water solvent.

Yield (730.4mg) with percentage yield = 76.85%, melting point (M.p)=230-233°C.

MS m/z 440.6 [M⁺=M-Cl], because of its monocationic nature [Cu(dpa)₂Cl]Cl, C₂₀H₁₈Cl₂CuN₆:

Calculated: C=50.38%; H= 3.80%; N= 17.62%.

Found: C=50.22%; H= 3.64%; N= 17.68%, FT-IR (νcm^{-1}): ($\nu\text{H-N}$)=3270, ($\nu\text{C-H}$ of pyridine)=3160, ($\nu\text{N-H}$)=1560, ($\nu\text{N-C}$)= 1180, ($\nu\text{Cu-N}$)= 610 and 520, UV-Visible spectra in water: λ_{max} =240nm, 320nm , 405nm , 675nm.

2.2 [Cu(dpa) (dien)]Cl₂ (4):

In 5 mL of distilled water (2mmol) of complex **3** was suspended under ultrasound waves, aqueous solution (4mL) of equivalent of dien (2mmol) was added drop wise to the solution under stirred and ultrasound waves atmosphere for 4minutes until the solution turned from green to blue; the volume of the solution was reduced to 1mL using vacuum.

Complex **4** was precipitated by adding 10mL of cooled methanol to the concentrated solution. The product was filtrated, then washed by *n*-hexane and dichloromethane, then dried under vacuum.

The complex was isolated as blue powder ,with:

Yield=(606.4mg) and percentage = 74.12%, melting point(M.p) =190-194°C.

MS m/z 338.4 [$M^+ = M - 2Cl$]. $C_{14}H_{22}Cl_2CuN_6$;

Calculated: C= 41.13%; H= 5.42% ; N=20.56%,

Found: C=41.03%; H=5.34%; N=20.33%.

FT-IR (νcm^{-1}): ($\nu\text{H-N}$) =3380 and 3250, ($\nu\text{C-H}$ of Pyridine)= 3155, ($\nu\text{C-H}$)= 2950,($\nu\text{N-H}$)= 1550, ($\nu\text{N-C}$)= 1160, ($\nu\text{Cu-N}$)= 605 and 530.

UV- Visible spectra in water λ_{max} at: 245nm, 310nm and 625nm.

3. Physical Measurements.

Elemental analyses were recorded with an Elementar Varrio EL- analyzer. The FT-IR spectra ($4000\text{-}400\text{cm}^{-1}$) were obtained from KBr- discs with a Perkin-Elmer 621 spectrophotometer.

Thermal analyses were carried out with TA instrument SDT-Q600 in air. Electronic spectra were recorded in water at room temperature on Pharmacia LKB-Biochrom 4060 spectrophotometer.

TOF-MS data were obtained a Finnegan 711A(8kV), modified by AMD and reported as mass/charge (m/z), respectively.

4. Single-Crystal X-Ray Data collection.

A suitable crystal of complex **3** was mounted with Epoxy on a glass fiber and the diffraction data was collected at room temperature using an Oxford X caliber diffractometer (Mo $K\alpha$ radiation, $\lambda = 0.7107 \text{ \AA}$).

Four sets of ω scans with a total of 237 frames of 29 s duration each were recorded. Data was reduced and processed to give *hkl* files using CrysAlisPro software [47].

The structures were solved by direct methods and refined by least-squares method on F^2 using the SHELXTL program package [48].

Except for the hydrogen atoms of the three interstitial water molecules the hydrogen atoms were placed in calculated positions and refined isotropically using a riding model. All non-hydrogen atoms were refined anisotropically, Details of crystal **3** data, and data collection and refinement are given in Table 2.

Table 2. Crystallographic Data and Structure Refinement Parameters of complex 3.

Complex 3 .	
Empirical formula	C ₂₀ H ₁₈ Cl ₂ Cu N ₆
Formula weight	476.84 g/mole
Temperature	293(2) K
Wavelength	0.71073 Å
Crystal system	Monoclinic
Space group	C12/c1
Unit cell dimensions	a = 22.8663(13)Å , α = 90°. b = 11.6802(6)Å , β = 117.861(7)°. c = 17.1019(10) Å , γ = 90°.
Volume	4038.2(4) Å ³
Z	8
Density (calculated)	1.569 Mg/m ³
Absorption coefficient	1.366 mm ⁻¹
F(000)	1944
Crystal size	0.3 x 0.2 x 0.1 mm ³
Theta range for data collection	2.96 to 26.29°.
Index ranges	-28 ≤ h ≤ 25, -14 ≤ k ≤ 9 , -21 ≤ L ≤ 20
Reflections collected	9119
Independent reflections	4095 [R(int) = 0.0326]
Completeness to theta = 26.29°	99.9 %
Absorption correction	Semi-empirical from equivalents
Max. and min. transmission	1.00000 and 0.79525
Refinement method	Full-matrix least-squares on F ²
Data / restraints / parameters	4095 / 0 / 262
Goodness-of-fit on F ²	1.033
Final R indices [I > 2sigma (I)]	R1 = 0.0369, wR2 = 0.0871
R indices (all data)	R1 = 0.0512, wR2 = 0.0970
Largest diff. peak and hole	0.755 and - 0.396 e Å ⁻³

Chapter Three

Results and Discussion

Chapter Three

PART1: Synthesis, Spectral and Structural of [Cu(1,10-phen)(dien)]Br₂(1) and [Cu(1,10-phen)(dipn)]Br₂(2)Complexes.

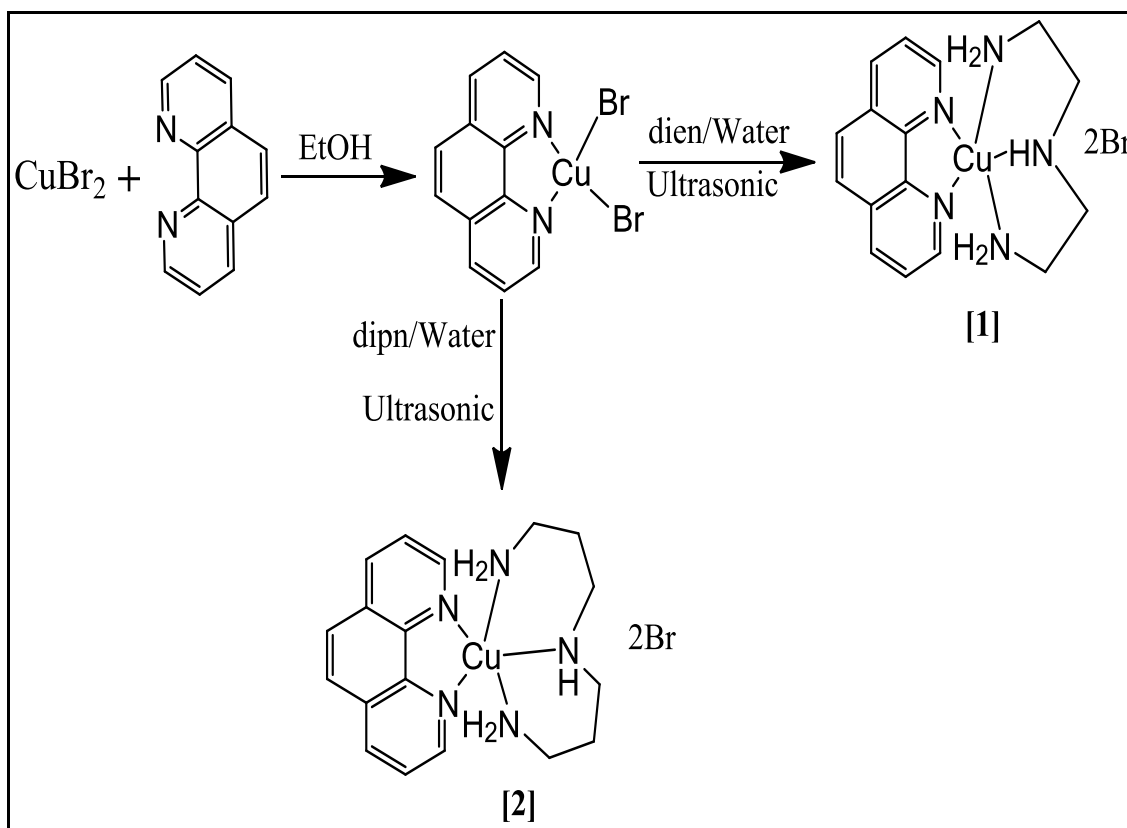
1. Introduction:

The design and synthesis of 1,10-phenanthroline metal complexes are fascinating areas of research due to their important applications [1, 2] as potential anti-tumor agents [3, 4]. Mixed-ligand complexes containing nitrogen donor ligands have been of special interest for many years because of their potential antimicrobial [1-4], antioxidant [5], anticancer and catalytic activities [6-9]. The photo-physical properties of Copper (II) complexes containing polypyridine ligands have shown to be useful as chemical probes for DNA [10-13]. It has been known that the anti-cancer activity of some copper(II) complexes may be based on their ability to inhibit DNA synthesis [16]. The determination of the structure of these complexes in solution is indispensable for the understanding of some biological processes [17, 18]. For example, neural copper complexes with chelating phenanthroline have hydrophilic groups which are act as potential anti-tumor agents because these complexes are expected to penetrate through the cell membrane [19-20], (dien) and (dipn) are tridentate nitrogen donor ligand with donor groups suitably placed for forming two five-membered chelate rings. Such tridentate ligands are known to form binuclear or trinuclear metal [21].

2. Synthesis of complexes 1 and 2 .

Mixed-ligand copper(II) complexes of the general formula $[\text{Cu}(\text{phen})(\text{NNN})]\text{Br}_2$ (**1-2**) [phen=1,10-phenanthroline, NNN= (dien) (**1**) and (dipn) (**2**)], were synthesized by the reaction of $[\text{Cu}(\text{Phen})\text{Br}_2]$ with NNN ligands under ultrasonic wave atmosphere as in (Scheme 1). These complexes have been isolated as bromide salts in good yields.

They have been characterized using elemental analysis and spectral methods. These complexes are blue in color and are soluble in water. The X-ray crystal structure of complex **1** reveals a distorted square pyramid to distorted trigonal bipyramidal geometry around Cu(II) ions.



Scheme 1. Syntheses of $[\text{Cu}(1,10\text{-phen})(\text{dien})]\text{Br}_2$ (**1**) and $[\text{Cu}(1,10\text{-phen})(\text{dipn})]\text{Br}_2$ (**2**) complexes.

3. IR Spectral Data.

The IR-KBr disk spectra of $\text{CuBr}_2(\text{phen})$ starting complex was compared to Complex **1** after dien addition as seen in figure(1). Only in complex **1** and **2** the peaks at 3420 cm^{-1} $\nu_{(\text{O-H})}$ (O–H) and 1426 cm^{-1} $\nu_{(\text{bend})}$ are the characteristic bands of H_2O which indicates the existence of molecular lattice water as in Figure 1.

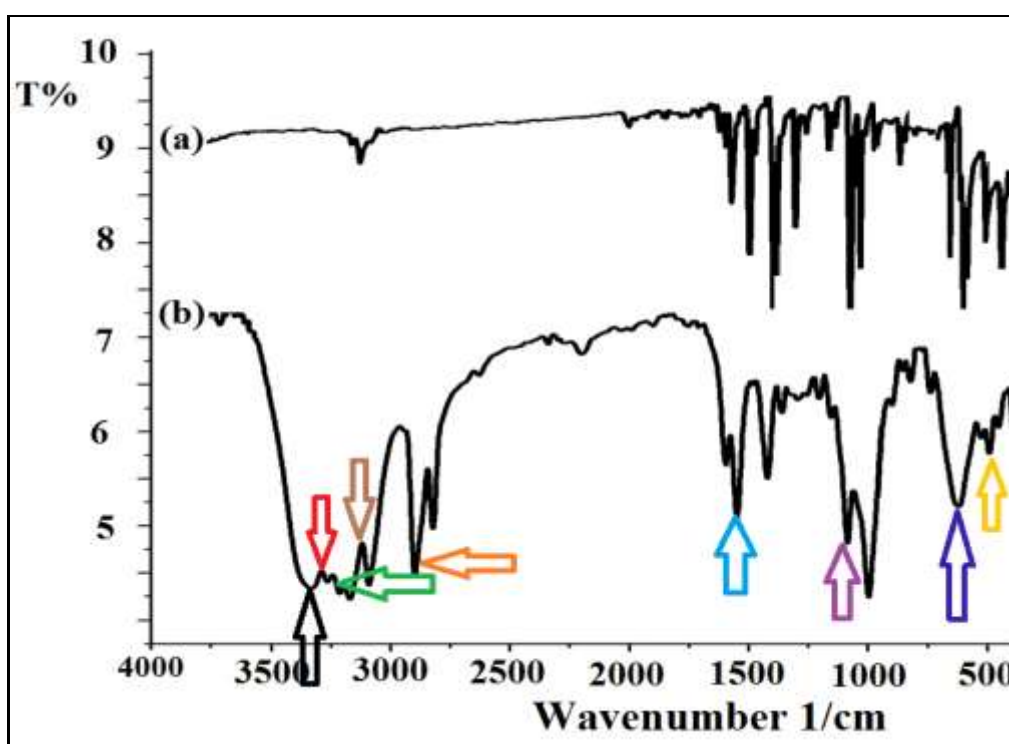


Figure 1. IR-KBr spectra of starting materials **a)** $[\text{CuBr}_2(1,10\text{-phen})]$, and **b)** $[\text{Cu}(1,10\text{-phen})(\text{dien})]\text{Br}_2$ (**1**).

In the spectra of the complexes **1** and **2** different in $[\text{CuBr}_2(\text{phen})]$ starting complex, the three bands at $3310\text{--}3413$, $3235\text{--}3266$ and $1583\text{--}1616\text{ cm}^{-1}$ assigned to $\nu_s(\text{N-H})$, $\nu_{as}(\text{N-H})$ and $\delta(\text{N-H})$, respectively are shifted to wave numbers lower than those encountered in the free triamine, confirming the coordination of the amine groups with copper [65].

The absorption band around 3140cm^{-1} is probably due to the stretching vibration of C-H phenylic bond [66]. The strong bands at around 2800-2950 cm^{-1} due to the stretching vibration of C-H of sp^3 hybridization alkyl in the triamine ligand [67].

As the lone pair of electrons of the donor nitrogen atoms become involved in the metal-ligand bond, the transfer of electron density to the metal and the subsequent polarization of the ligands involves electron depopulation of the N-H bond, which culminates in a shift to lower frequencies [68, 69]. Appearance of a band at 510cm^{-1} was due to $\nu(\text{Cu-N})$ vibrations [70], a band appeared in the $292\text{-}295\text{cm}^{-1}$ region was assigned to the $\nu(\text{Cu-Br})$ vibration [71].

The spectral wave number of complex **2** band assigned vibration and stretching $3440\text{ cm}^{-1}(\nu\text{H}_2\text{O})$, 3317 cm^{-1} , 3360 cm^{-1} and $3270\text{ cm}^{-1}(\nu\text{H-N})$, 3160 cm^{-1} ($\nu\text{ C-H}$ of phenyl), 2940 cm^{-1} ($\nu\text{ C-H}$), 1560 cm^{-1} , 1448 cm^{-1} ($\nu\text{N-H}$), 1180 cm^{-1} , 1113 cm^{-1} ($\nu\text{N-C}$), 610 cm^{-1} and $520\text{ cm}^{-1}(\nu\text{ Cu-N})$.

4. Thermal Analyses (TGA / DTA).

The thermal stabilities of the complexes were investigated by TG/DTA, The TGA curves were obtained at a heating rate of $10^\circ\text{C min}^{-1}$ in air atmosphere over the temperature range of $25\text{-}1000^\circ\text{C}$. The thermogravimetric analyses of these complexes revealed the occurrence of three consecutive processes, namely dehydration, ligand pyrolysis and inorganic residue formation .

The desired Cu(II) complexes showed similar thermo-gravimetric behavior, the TG/DTA spectra of complex **2** illustrated mainly the expected three steps of weight loss as in Figure 2

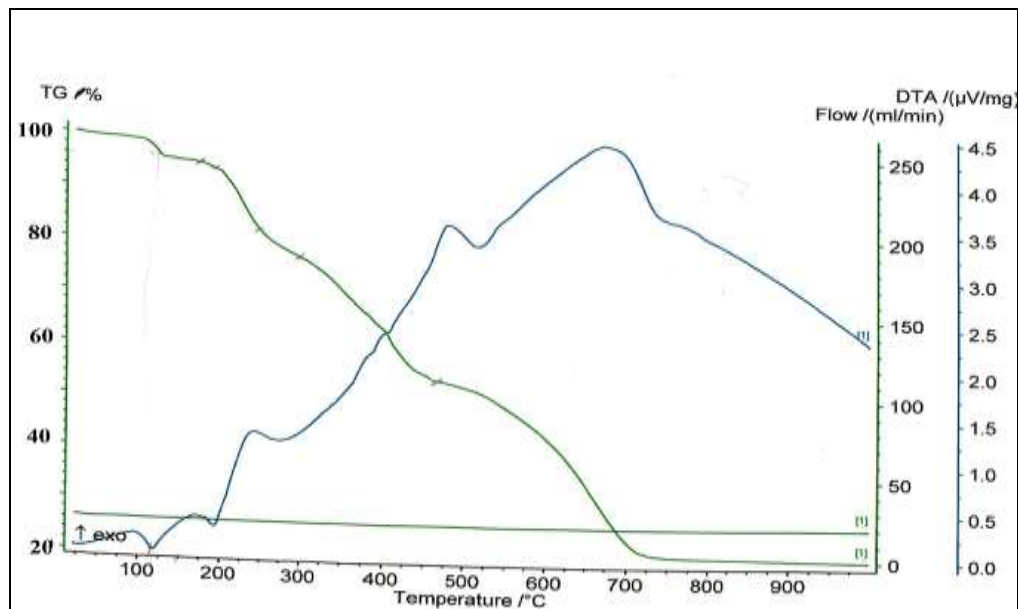


Figure 2. Thermo-gravimetric (TG/DTA) analysis of Cu(1,10-phen)(dipn)Br₂ (**2**).

The first step was losing uncoordinated water molecule at endothermic sign of DTA at 107 °C .

The second decomposition stage from 160 °C and end at 480 °C losing around 40% of weigh, triamine lose with two DTA exothermic signs at 250 and 480 °C with expected final product of this step is CuBr₂.

The third step starts from 480 °C and end at 720 °C which lead to the removal of bromide ions of CuBr₂ to form copper oxide (Cu=O) final product with sharp weight loss.

The final residue was analyzed by IR spectra and identified as Copper oxide (CuO = 22%).

5. Crystal structure for complex 1 .

Complex 1 crystallizes in the Monoclinic P121/n1space group. The crystal data and structure refinement parameters are given in Table 1 and selected bond distances and bond angles are given in Table 3 and 4 .

Table 3. Experimental X-Ray and calculated bond length of complex 1 by Time Dependent-Functional Theory.

<u>Major bond length of chemical complex formed:</u>	<u>Experimental [Å]</u>	<u>Calculated [Å]</u>
Cu(1)-N(10)	2.212(4)	2.267
Cu(1)-N(3)	2.035(3)	2.088
Cu(1)-N(1)	2.030(4)	2.066
Cu(1)-N(4)	2.019(4)	2.075
Cu(1)-N(5)	2.016(4)	2.088

Table 4. Major Bond angle (N-Cu-N) for complex 1

<u>Major chemical Bond angles:</u>	<u>Measured. [°]</u>	<u>Calculated. [°]</u>
N(5)-Cu(1)-N(4)	84.15(14)	83.19
N(4)-Cu(1)-N(1)	175.09(16)	171.98
N(5)-Cu(1)-N(3)	155.92(15)	155.81
N(4)-Cu(1)-N(3)	84.36(14)	83.14
N(1)-Cu(1)-N(3)	94.01(15)	95.39
N(5)-Cu(1)-N(10)	109.64(14)	101.84
N(4)-Cu(1)-N(10)	105.85(16)	109.78
N(1)-Cu(1)-N(10)	78.86(16)	78.23
N(3)-Cu(1)-N(10)	93.85(14)	101.54
N(5)-Cu(1)-N(1)	95.65(15)	95.34

The ORTEP diagram of the molecule with the atomic numbering is shown in Figure 3. Interestingly, the Cu²⁺ ion in complex 1 is coordinated by two N atoms of one phen ligand and three N atoms of one triamine ligand, yielding mixed coordinated complex cation [Cu(phen)(triamine)]²⁺.

The 5-fold coordinated Cu^{2+} ion is in a distorted trigonal bipyramidal environment with $\text{Cu-N10} = 2.212(4) \text{ \AA}$ and one shorter basal site with $\text{Cu1-N1} = 2.030(4) \text{ \AA}$. The three other basal sites are occupied by N atoms from dien with Cu1-N of $2.016(4)$, $2.019(3)$ and $2.035(3) \text{ \AA}$. The structural features of the present compounds are very similar to reported $[\text{Cu}(\text{dien})(\text{phen})](\text{ClO}_4)_2$ [72], with one of the two N atoms of phen occupying the apical site $\text{Cu-N}(\text{apical}) = 2.186 \text{ \AA}$, and the other basal site $\text{Cu-N}(\text{basal}) = 2.022 \text{ \AA}$.

For complex **1** the geometry around the copper(II) ion can be best described as trigonal bipyramidal distorted to square based pyramidal as indicated by the value of the trigonal index $\tau = 0.25$ for complex **1** where $(\tau = \beta - \alpha / 60)$, where α and β are the largest coordination angles are the largest coordination angles.

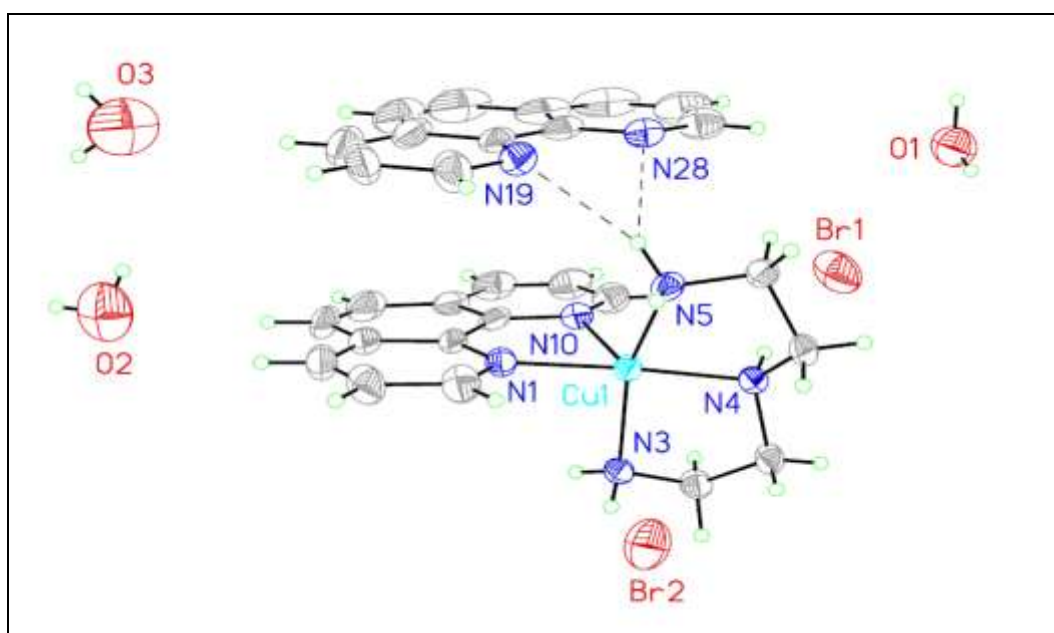


Figure 3. The ORTEP generated diagram of complex **1** with displacement ellipsoids drawn at 50% probability level.

The value of τ is one for perfect trigonal bipyramidal geometry and is zero for a perfect square pyramidal geometry [73]. The disposition of the uncoordinated phen is basically parallel to the Cu bonded phen with dihedral angle between the planes of both of 2.40° as is shown in the crystal packing structure Figure 7. The uncoordinated phen is linked to the coordinated complex *via* N-H...N hydrogen bonding interactions and N(π)...N interactions.

The N-H...N bifurcated hydrogen atom bonding interactions are listed in Table 5 and Figure 4, 5, 6. This arrangement is reinforced by N(π)...N interactions; N(π) is electron deficient π -system around positively charged nitrogen atom.

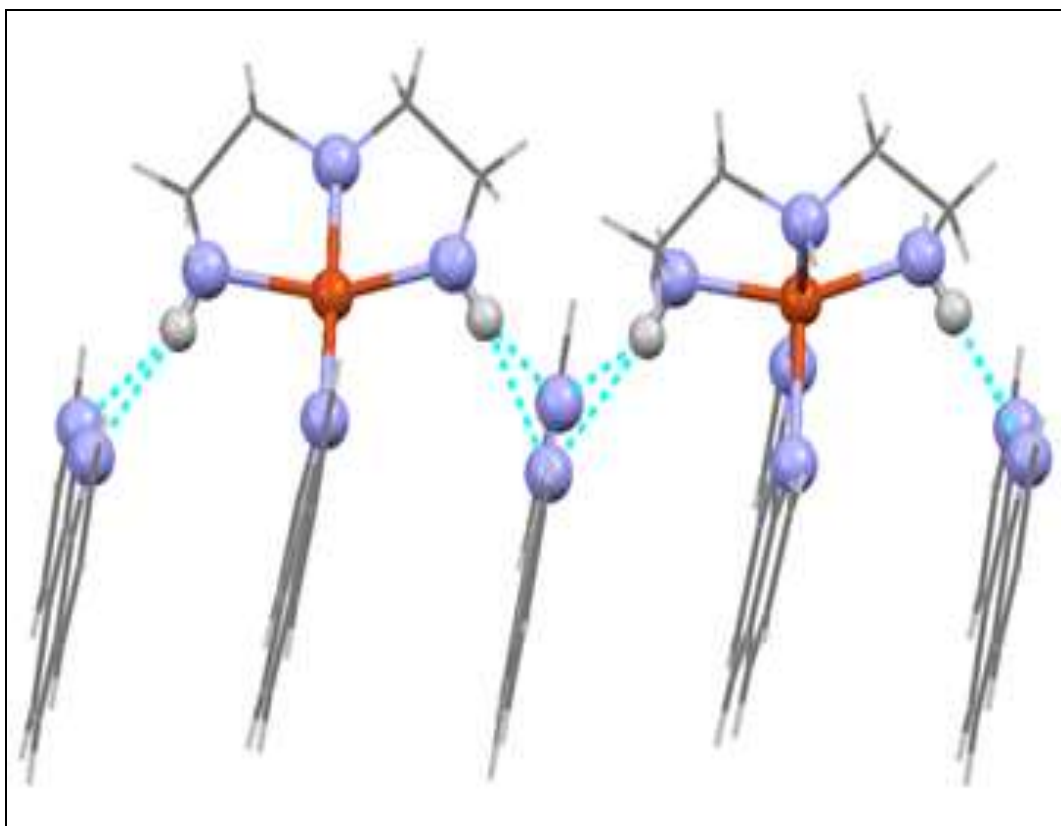


Figure 4. Chain structure of complex 1.

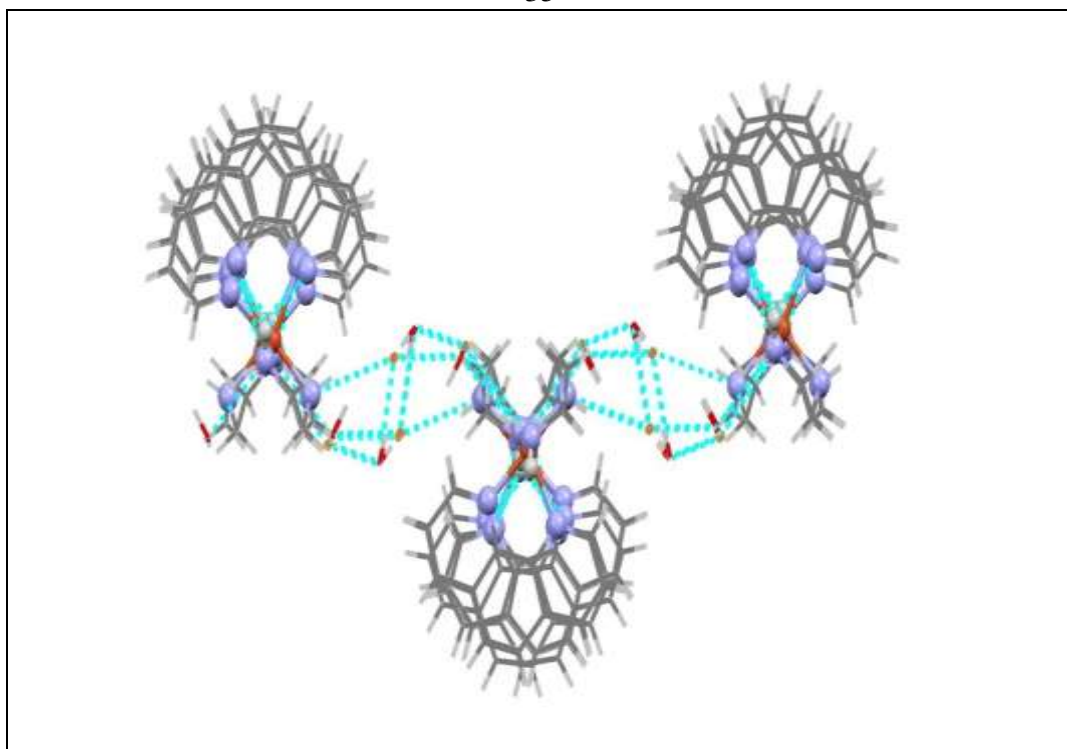


Figure 5.The layer structure of the complex 1.

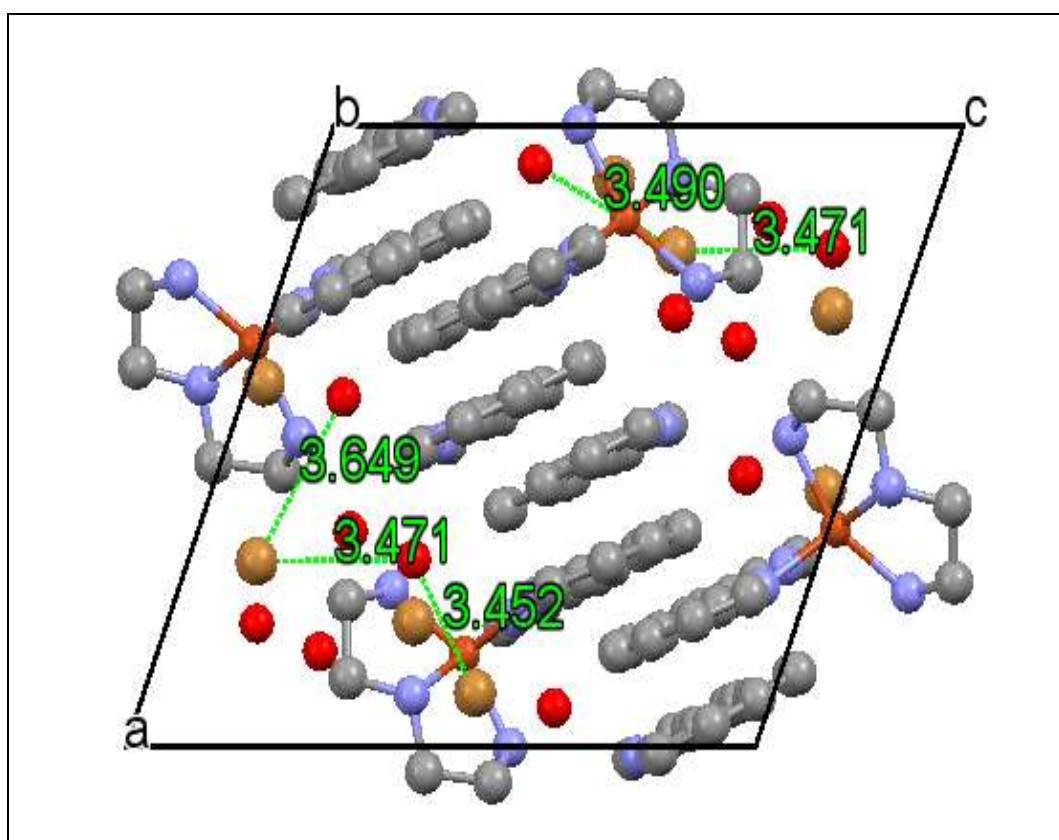


Figure 6.Chain structure of complex 1 and crystal packing .

Figure 7 indicates clearly that the electron rich N atom of the phen free ligand is located above the electron deficient $N(\pi)$ system of complexation. The $N(\pi)\dots N$ distances are 3.665 Å and 3.755 Å for $N1(\pi)\dots N19$ and $N10(\pi)\dots N28$. have shown that these interactions play a crucial role in the self-assembly of many mixed organic-inorganic hybridized materials [74, 75] .

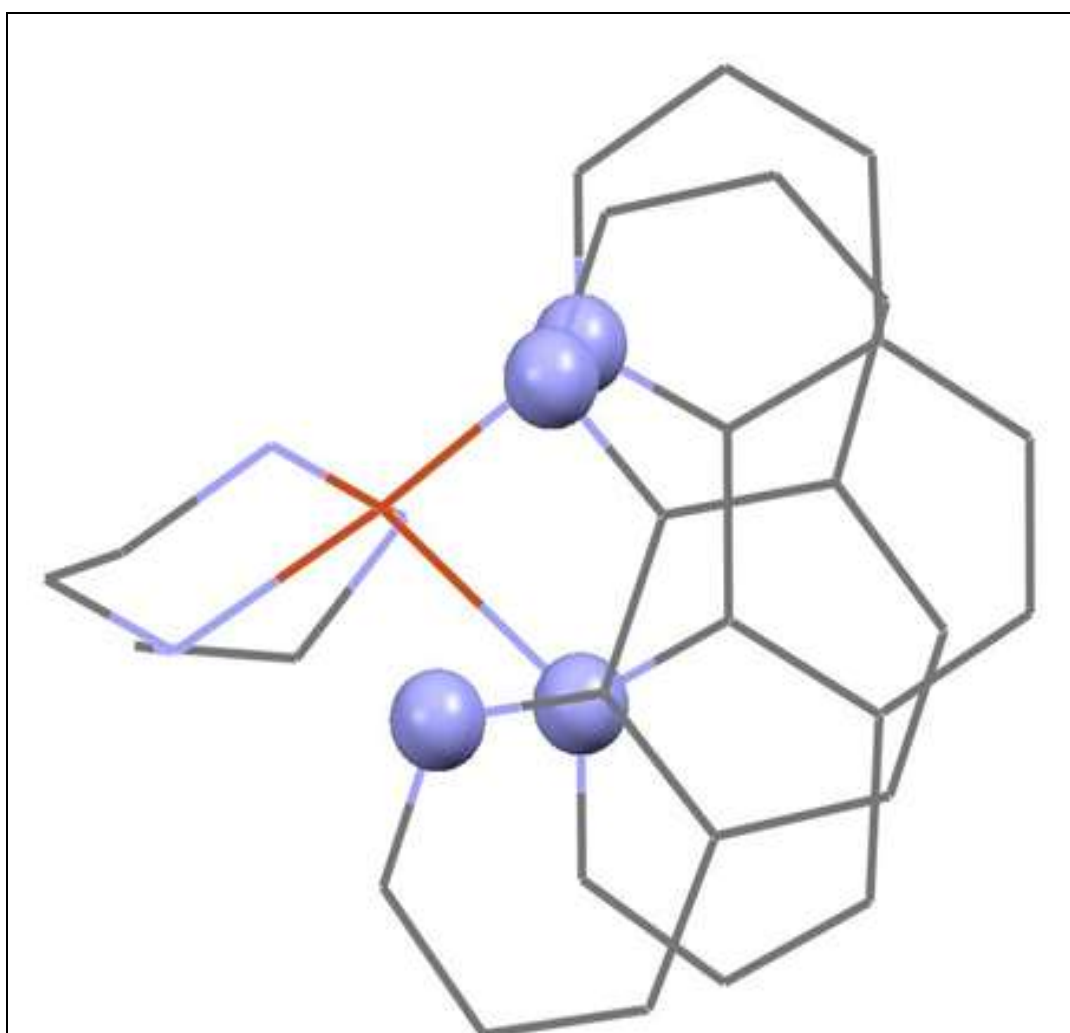


Figure 7. Illustration of the $N(\pi)\dots N$ interactions. View is perpendicular to the plane of the aromatic systems. All atoms are represented as wire frames except nitrogen atoms that are involved in the interactions as spheres .

Table 5. Hydrogen bonds distances (Å) and angles (°).

D-H [Å]	A	d(H..A) [Å]	d(D..A) [Å]	[°]<DHA
N5-H5'A	N19	2.338	3.162	152.18
N5-H5'A	N28	2.547	3.287	139.94
N5-H5'B	O1 ^a	2.104	2.954	157.06
N3-H3'A	Br2	2.713	3.468	142.21
N3-H3'B	N19 ^b	2.461	3.266	148.96
N3-H3'B	N28 ^b	2.521	3.241	137.43
N4-H4'A	Br1	2.622	3.499	161.83
O2-H21	O3	2.591	3.413	151.55
O3-H32	Br1 ^c	2.705	3.466	142.37
O2-H22	Br1 ^c	2.987	3.648	131.67
O2-H22	Br1 ^d	3.057	3.536	115.17
O1-H12	Br2 ^e	2.518	3.391	163.36
^a [-x+3/2,y+1/2,-z+1/2], ^b [x-1/2,-y+1/2,z-1/2], ^c [x+1/2,-y+1/2,z-1/2], ^d [-x+3/2,y+1/2,-z-1/2], ^e [-x+3/2,y-1/2,-z+1/2].				

The three water molecules of hydration are hydrogen bonded to the two Br⁻ ions in the asymmetric unit as is shown in Figure 3, the packing diagram. The water O and Br⁻ vary in distance between 3.452 and 3.649 Å. The N-H...N and N(π)...N interactions connect the cationic complex and the free phen ligand to form a chain structure in run 101 direction.

These chains are linked *via* N-H...Br, N-H...O and O-H...Br hydrogen bonding interactions to form a layer structure lies parallel to the 1-0-1 plane. Subsequently, these chains interdigitate to form the dimensional structures via weaker interactions non-classical hydrogen bonding interactions C-H...O and C-H...Br. These interactions are not analyzed since C-H groups are abundant in the crystal structure.

6. UV-Visible and ultraviolet spectra.

UV-visible electronic absorption spectrum of complex **1** and **2** and the starting material complex $\text{CuBr}_2(1,10\text{-Phen})$ were measured in H_2O at room temperature. The blue shift in λ_{max} by $\cong 85\text{nm}$ in absorption spectrum of complex **1** after (dien) ligand addition to $[\text{CuBr}_2(\text{phen})]$ from $\lambda_{\text{max}}=705\text{nm}\rightarrow 620\text{nm}$, and the same as in complex **2** absorption spectrum blue shift in λ_{max} by $\cong 95\text{nm}$ after addition (dipn) ligand from $\lambda_{\text{max}}=705\text{nm}\rightarrow 610\text{nm}$ this confirm the N-tridentate ligand make coordination with starting complex $[\text{CuBr}_2(\text{Phen})]$ to synthesize the desired complexes as shown in Figure **8, 9**.

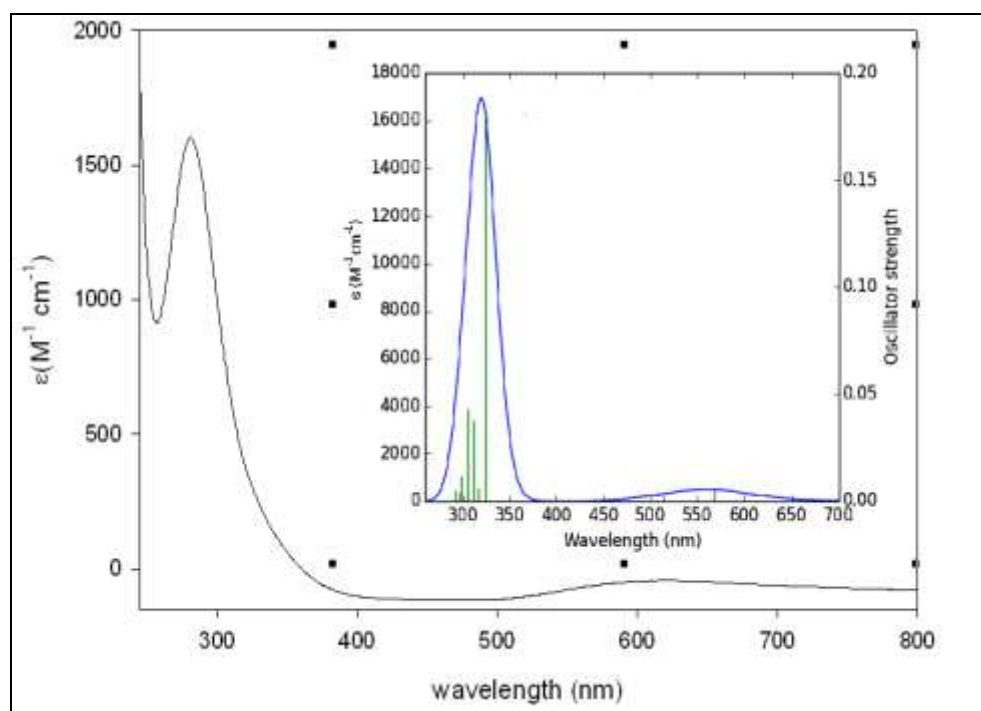


Figure 8. UV-Visible spectra of complex **1** in water at room temperature (RT).

The electronic spectrum of complex **1** and **2** in revealed similar electron transfer showing a peak $\lambda_{\text{max}} \cong 280\text{ nm}$ and 282 nm were assigned to intra-ligand π to π^* electron transitions of the phenanthroline ligand, this region

of absorption was also detected in $[\text{Cu}(\text{Phen})\text{Br}_2]$ complex which has a red shift by $\approx 15\text{nm}$ and 17nm compared with free phen ligand at $\lambda_{\text{max}} \approx 265\text{nm}$, while the less intense band at $\approx 380\text{ nm}$ for complex **1** and **2** was assigned for ligand to metal charge transfer (LMCT) transitions.

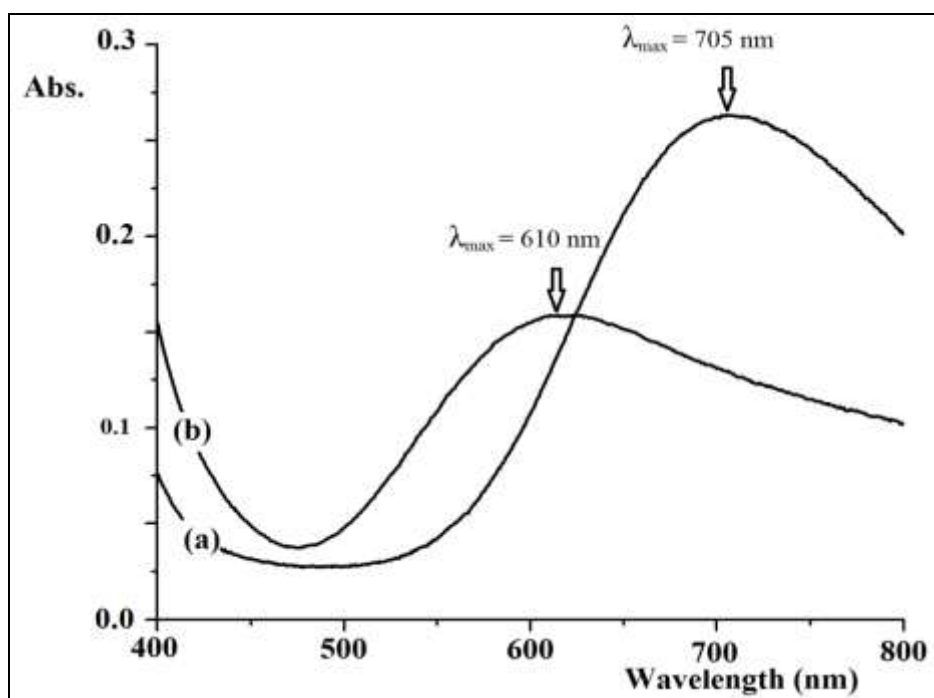


Figure 9. UV-Visible spectra of **(a)** $\text{CuBr}_2(1,10\text{-phen})$ addition **(b)** complex **2**, dissolved in water at room temperature (RT).

Additionally, much intense well defined d-d broad bands transitions observed in the lower energy regions at 705nm in $[\text{CuBr}_2(\text{Phen})]$ starting complex before addition N-tridentate ligand, and after addition of triamine(dien and dipn) ligand, this shift confirms the N-tridentate coordination as well as represent a distorted square pyramidal geometry around Cu(II) ions.

TD-DFT calculations have been performed for complex **1**. The full geometry optimizations for compounds have been carried out at the

DFT/B3LYP level. Some selected optimized bond parameters for complex **1** are given in Table 3 and 4. The optimized bond lengths and angles well reproduced the X-ray data of the complexes. Contour plots of some selected molecular orbitals are shown in the Figure 10, Energy and compositions of some selected molecular orbitals are given in supplementary Table 6.

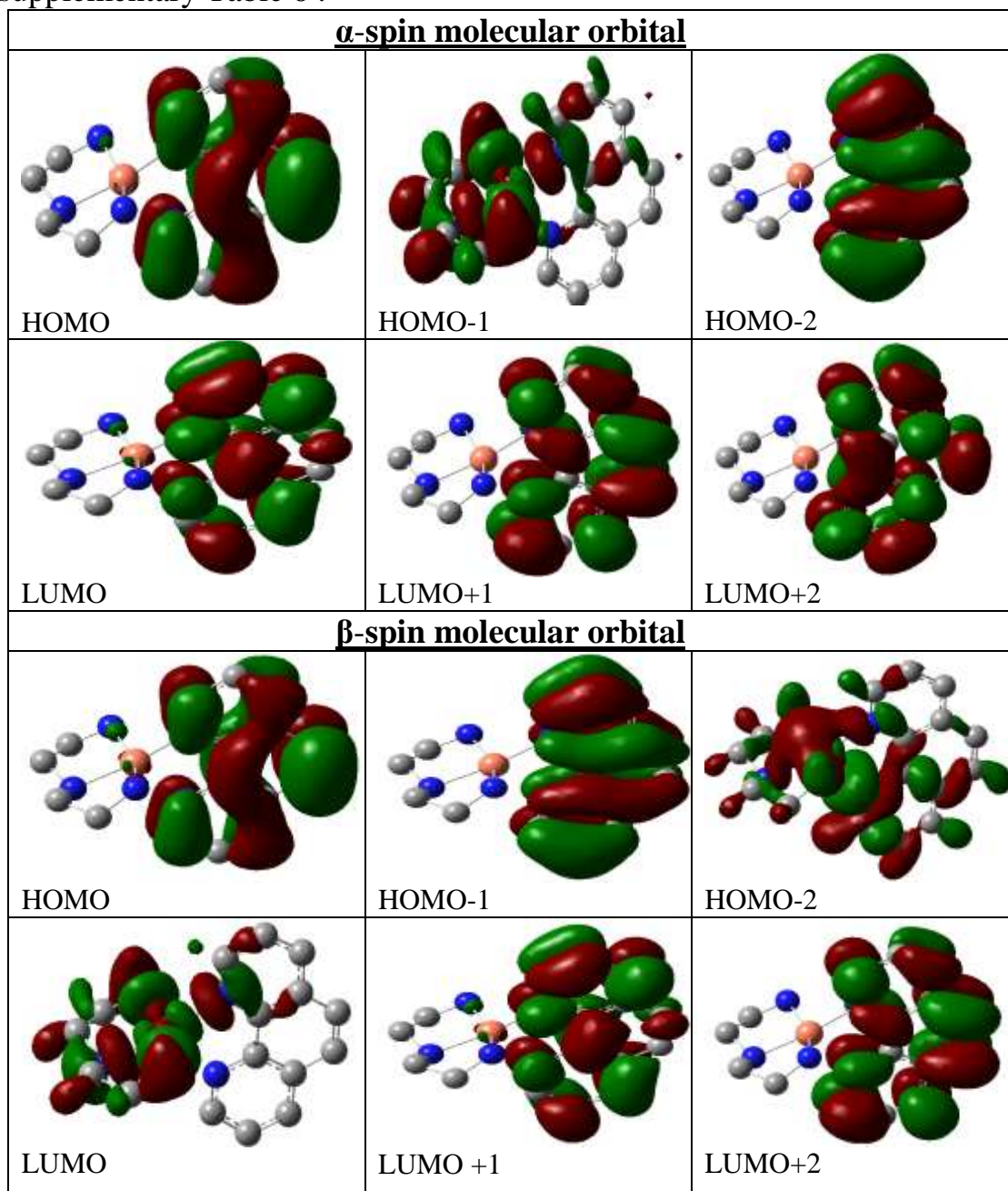


Figure 10. Isodensity plots of some selected MOs (α -spin and β -spin) of complex **1**.

Table 6. DFT energies and composition of selected highest occupied (H) and lowest unoccupied (L) molecular orbitals of complex 1 expressed in terms of composing fragments for complex.

α - MO					β - MO				
MO	eV	phen	Cu	Triamine	MO	eV	phen	Cu	triamine
L+4	-0.03	2	80	17	L+3	-1.18	99	1	1
L+3	-0.43	99	1	0	L+2	-2.34	100	0	0
L+2	-1.18	99	1	0	L+1	-2.53	98	1	0
L+1	-2.33	100	0	0	L	-3.88	9	58	33
L	-2.56	98	1	0	H	-7.12	99	0	1
H	-7.13	99	0	0	H-1	-7.52	100	0	0
H-1	-7.51	18	19	64	H-4	-8.79	30	11	59
H-2	-7.53	100	0	0	H-7	-9.77	59	31	10
H-3	-8.13	67	23	11	H-9	-10.04	64	20	17
H-4	-8.92	57	6	36	H-10	-10.16	30	48	22
H-7	-9.14	43	7	49	H-11	-10.24	15	68	16
					H-13	-10.48	15	42	43
					H-16	-10.89	7	76	17

For complex 2, the β -spin occupied orbitals mainly take part for the electronic transitions in the visible while a mixture of α and β -spin are responsible for the electronic transition in the UV-region. The β -spin for LUMO is composed mainly from Cu (58%) and triamine ligand (33%) while LUMO+1 to LUMO+5 mainly phenanthroline in character Table 6. The β -spin for HOMO to HOMO-6 is mainly phenanthroline in character and HOMO-7 to HOMO-15 has a Cu and triamine character. The spin for HOMO-7 to LUMO+3 are mainly phenanthroline in character.

Computation of 20 excited states of complex 1 and 2 allowed the interpretation of the experimental spectra of the complex in the 200→800 nm range Figure 8 and 9 The calculated energy of excitation states and transition oscillator strength (f) are shown in Table 7. The absorption

spectrum of complex **2** was simulated using Gauss Sum software [64] based on the obtained TD-DFT results. Both the experimental Ultra violet and Visible spectra and its simulated absorption spectra in water shown in Figure **9** and **10** are in acceptable agreement.

Table 7: Computed excitation energies λ (nm), electronic transition configurations and oscillator strengths (f) for the optical transitions in the visible region of complex (1) transitions with $f \geq 0.004$ are listed.

λ (nm)	f	Composition
568.9	0.0057	HOMO-16(β) \rightarrow LUMO (β) (12%), HOMO-10(β) \rightarrow LUMO (β) (18%), HOMO-9(β) \rightarrow LUMO (β) (15%), HOMO-3(β) \rightarrow LUMO (β) (27%), HOMO (β) \rightarrow LUMO (β) (18%).
512.7	0.0022	HOMO-13(β) \rightarrow LUMO (β) (18%), HOMO-11(β) \rightarrow LUMO (β) (53%), HOMO-7(β) \rightarrow LUMO (β) (12%).
323.9	0.1822	HOMO-4(β) \rightarrow LUMO (β) (72%).
316.4	0.0058	HOMO (α) \rightarrow LUMO (α) (35%), HOMO-4(β) \rightarrow LUMO (β) (15%), HOMO (β) \rightarrow LUMO+1(β) (35%).
311.2	0.038	HOMO-1(α) \rightarrow LUMO (α) (34%), HOMO-3(β) \rightarrow LUMO (β) (34%).
304.9	0.0431	HOMO-1(α) \rightarrow LUMO (α) (36%), HOMO-3(β) \rightarrow LUMO (β) (23%).
298.5	0.0119	HOMO-2(α) \rightarrow LUMO (α) (18%), HOMO (α) \rightarrow LUMO+1(α) (30%), HOMO-1(β) \rightarrow LUMO+1(β) (19%), HOMO (β) \rightarrow LUMO+2(β) (29%).

PART2:Synthesis, Spectral and Structural of [Cu(2,2'-dpa)₂ Cl]Cl (3) and [Cu(2,2'-dpa)(dien)]Cl₂ (4) Complexes.

1. Introduction:

The coordination chemistry of 2,2'-dipyridylamine (dpa) ligand and its derivatives has now been the subject of a number of several studies, due to their affinity and coordination versatility for most of metal ions [1-5].

dpa is an aromatic amine behaves mostly as a neutral or monoanionic or bidentate ligand [3-5]. The N-H group is usually not involved in coordination because of geometrical constraints and the two pyridine rings are flexible in their coordination to metal centers, leading to different coordination modes such as monodentate, chelating bidentate and bridging tridentate [9-12].

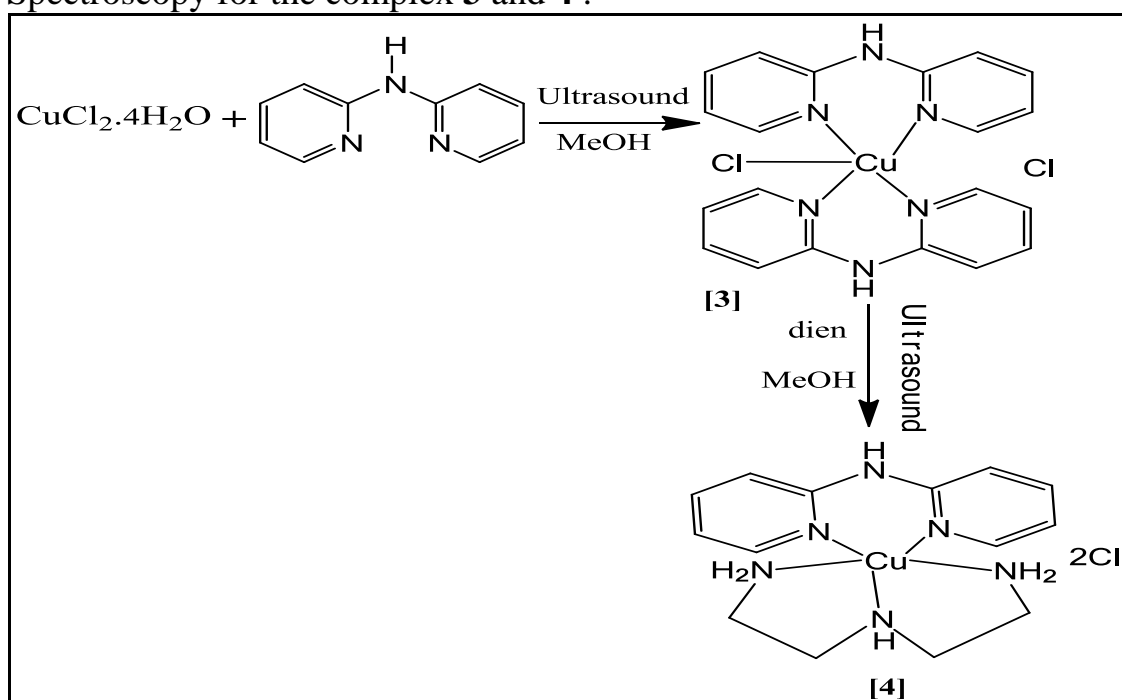
In mononuclear dipyrldylamine complexes behaves as a bidentate chelating ligand bonded through both the terminal pyridine nitrogen donor sites [13]. Further, the amine proton of dpa becomes more acidic upon complexation to the metal center, both form of the protonated and deprotonated (dpa) metal complexes are known [14-16]. The deprotonated form believed to result in form a planar ligand configuration in their metal complexes [16].

2. Synthesis of complex 3 and 4 .

Water soluble monocationic Complex 3 [Cu(dpa)₂Cl]Cl was made available by reacting two equivalent amount of dpa ligand with hydrated

CuCl_2 in methanol. $[\text{Cu}(\text{dpa})(\text{dien})]\text{Cl}_2$ complex **4** was prepared by reacting equivalent amounts of complex **3** with dien ligand in methanol.

The color changed from green to blue indicate the formation of complex **4**. The conductivity and solubility of **4** in water are twice higher than **3** which supported the dicationic and monocationic formation respectively as shows in (Scheme 2). These complexes have been isolated as chloride salts in a good yields. They have been characterized using elemental analysis and spectral methods. The structure of complex **3** confirmed and solved by single crystal X-ray with distorted square pyramid geometry and Mass Spectroscopy for the complex **3** and **4**.



Scheme 2. Synthesis $[\text{Cu}(\text{2,2}'\text{-dpa})_2\text{Cl}]\text{Cl}$ (**3**) and $[\text{Cu}(\text{2,2}'\text{-dpa})(\text{dien})]\text{Cl}_2$ (**4**) complexes.

3. IR Spectral Data.

In the spectra, the three bands at $3310\text{--}3413\text{cm}^{-1}$, $3235\text{--}3266\text{cm}^{-1}$ and $1583\text{--}1616\text{cm}^{-1}$ complexes **3** and **4** are assigned to $\nu_s(\text{N-H})$, $\nu_{as}(\text{N-H})$ and

$\delta(\text{N-H})$, respectively. These bands are shifted to lower wave numbers upon coordination relative to the free dien ligand, confirming the coordination of the amine groups with copper [65].

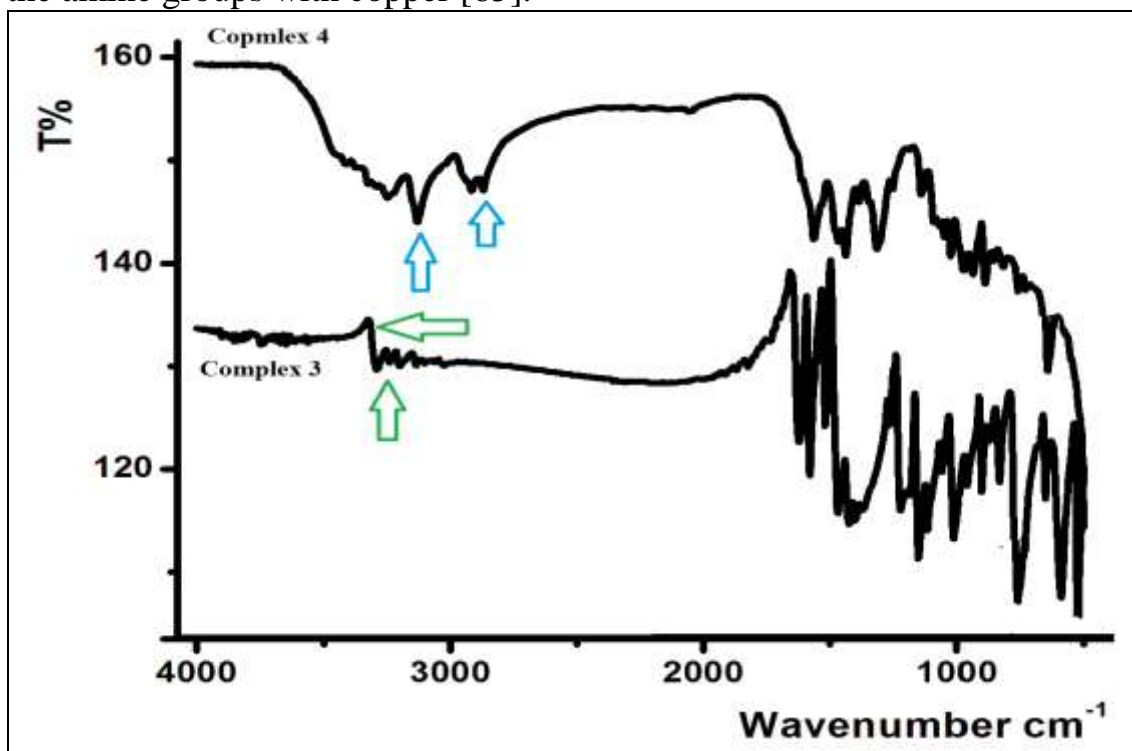


Figure 11. FT-IR spectra of complex 3 ,and complex 4 of copper(II) chloride.

In both complexes the absorption band around 3140 cm^{-1} is probably due to the stretching vibration of C-H pyridine bond [66]. In complex 4 only strong bands around $2800\text{-}2950\text{ cm}^{-1}$ due to the stretching vibration of C-H of sp^3 hybridizations alkyl of the dien ligand was observed [67]. Appearance of a band around $700\text{-}500\text{ cm}^{-1}$ was due to $\nu(\text{Cu-N})$ vibrations [66,85]. A band appeared in the $290\text{-}200\text{ cm}^{-1}$ region was assigned to the $\nu(\text{Cu-Cl})$ vibration [71, 84] as in Figure 11 .

4. TGA/DTA and Mass Spectroscopy .

4.1 Thermal analysis (TGA/DTA):

The thermal stabilities of the complexes were investigated by TGA/DTG. The TG curves were obtained at a heating rate of $10\text{ }^{\circ}\text{C min}^{-1}$ in open atmosphere over the temperature range of 0–1000 $^{\circ}\text{C}$.

The Thermogravimetric analyses of these complexes revealed the occurrence of two consecutive processes, ligands pyrolysis and inorganic residue formation. Complexes showed similar thermogravimetric behavior, no uncoordinated or coordinated water was detected in the lattice of these complexes.

The TG/DTG spectra of complex **3** illustrated mainly the expected two steps of weight loss:

First step was losing of two dpa ligands stage from 280 $^{\circ}\text{C}$ and end at 440 $^{\circ}\text{C}$ losing around 68% of weigh to form CuCl_2 .

The second step starts from 580 $^{\circ}\text{C}$ and end at 660 $^{\circ}\text{C}$ which lead to the removal of chloride ion of CuCl_2 to form copper oxide 19% as in **Figure12a**.

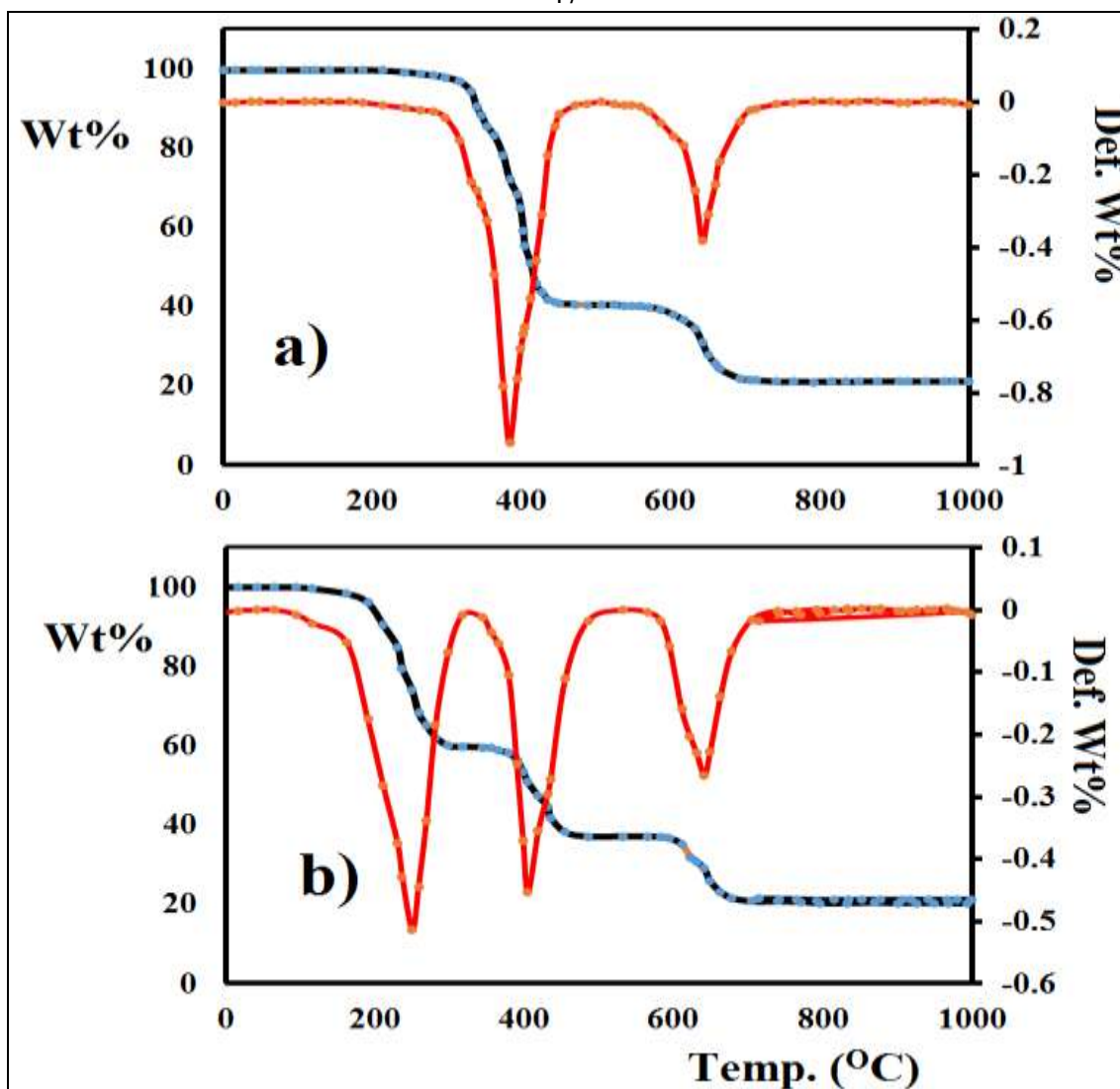


Figure 12. TG/DTG Thermal curves of the (a) complex 3, and (b) complex 4 .

The TG/DTG spectra of complex 4 illustrated mainly three steps of weight loss:

First step was losing of dpa ligand stage from 200°C and end at 380°C losing around 42% of weigh.

The second decomposition stage from 380°C and end at 460°C losing around 26% of weigh due to dien with expected final product CuCl_2 .

The third step starts from 580 °C and end at 660 °C which lead to the removal of chloride ions of CuCl_2 to form copper oxide final product with sharp weight loss as in Figure12b .

The final residue of both complexes were analyzed by FT-IR spectra and identified copper oxide(Cu=O), 20%) as in Figure13 .

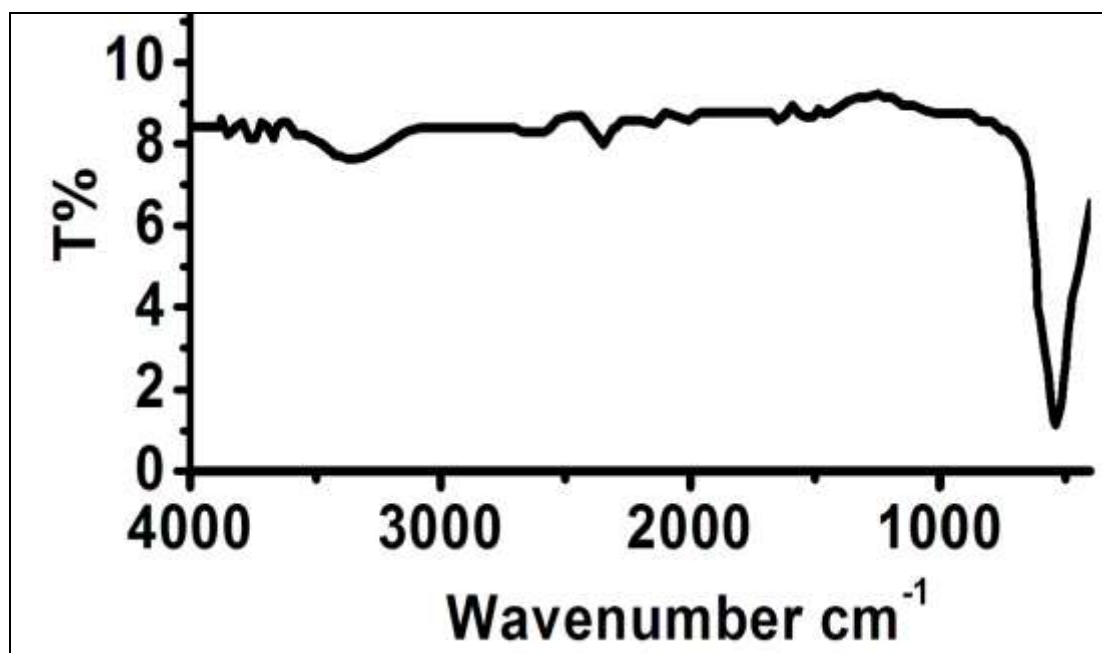


Figure 13. FT-IR spectra of (Cu=O) residues.

4.2 TOF-Mass spectra:

Time of flight MS is confirmed by the molecular ion peak at $m/z = 440.2$ (theoretical 440.6) for complex **3** $[\text{Cu}(\text{dpa})_2\text{Cl}]\text{Cl}$, and 338.4 (theoretical 337.2) for complex **4** $[\text{Cu}(\text{dpa})(\text{dien})]\text{Cl}_2$, as seen in Figure 14 .

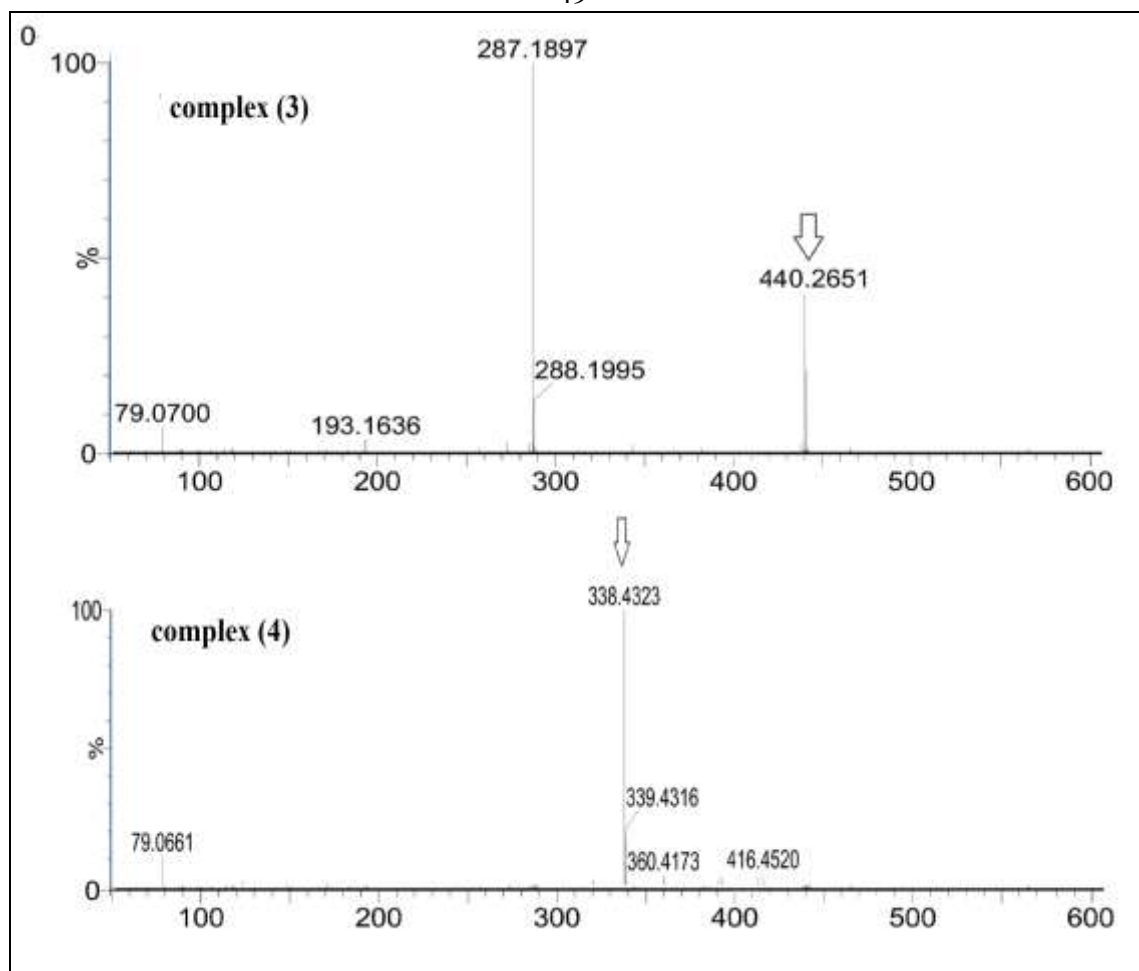


Figure 14. TOF-MS spectra of complex **3** [Cu(dpa)₂Cl]Cl and complex **4** [Cu(dpa)(dien)]Cl₂.

5. UV-visible and ultraviolet spectra.

Preparation of complex **4** from complex **3** was easily detected by eye due to the visible changes in colors by addition of dien ligand, the ligands substitution reaction was monitored by UV-visible spectrophotometric in H₂O at room temperature.

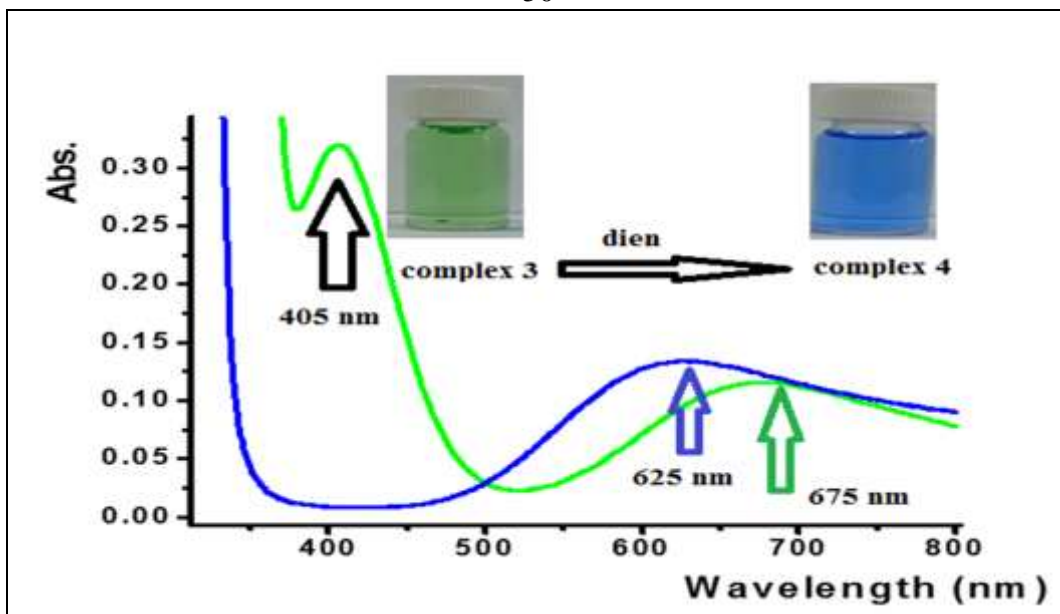


Figure 15. UV-Visible spectra of $[\text{Cu Cl} (2,2'\text{-dpa})_2]\text{Cl}$ (**3**) and $[\text{Cu}(2,2'\text{-dpa})(\text{dien})]\text{Cl}_2$ (**4**) dissolved in water at RT.

In the visible region, complex **3**, **4** (10^{-4}M) exhibited two sharp absorption maximums at 405 and 675nm can be assigned to MLCT and d-d electron transitions, respectively [46, 85].

When dien ligand was added to complex **3**, only one broad peak absorption maximum at 625nm was observed (blue).

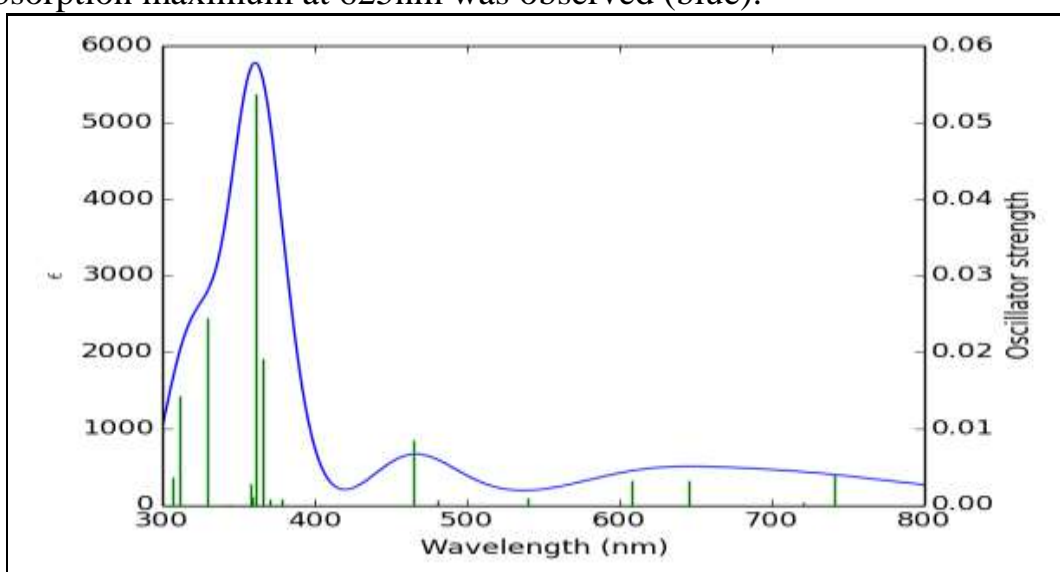


Figure 16. The Calculated UV-Vis spectrum of complex **3** in water.

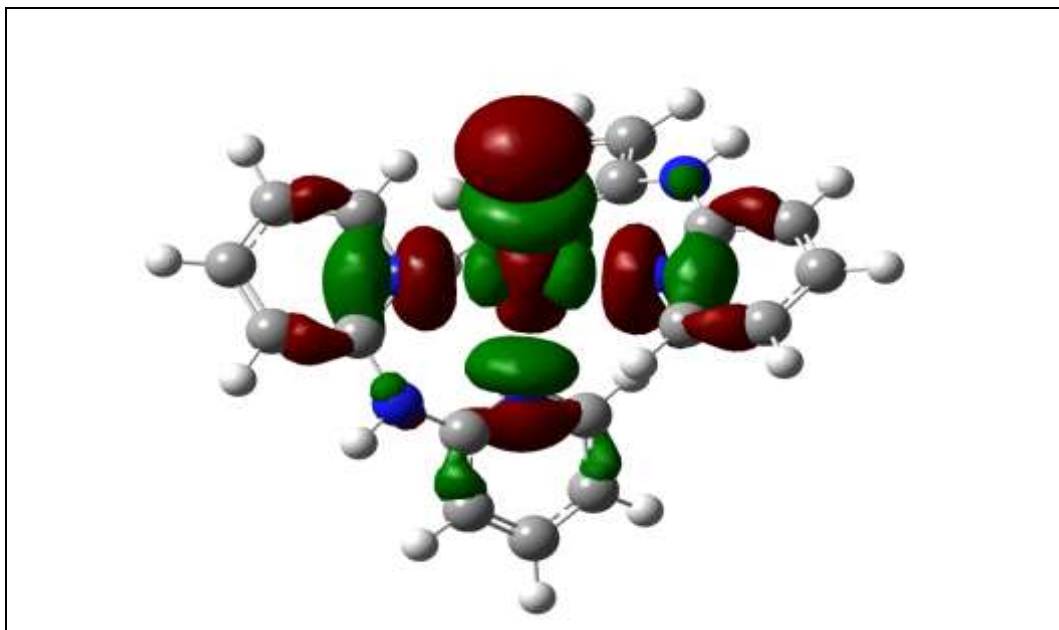


Figure 17. β - LUMO molecular orbital of complex 3 .

Table 8 .Calculated absorption wavelength, oscillator strength and molecular orbital contributions of UV-Vis electronic transitions, transitions with oscillator strength less than 0.02 are not listed.

Wavelength (nm)	Oscillation Strength	Major contributors
741.5271	0.004	H-4(β) \rightarrow L(B) (15%), H(β) \rightarrow L(β) (53%).
645.7465	0.0032	H-4(β) \rightarrow L (β) (16%), H-3(β) \rightarrow L(β) (13%), H-2 (β) \rightarrow L(β) (16%) , H(β) \rightarrow L(β) (32%).
608.0893	0.0032	H-2(β) \rightarrow L(β) (38%), H-1(β) \rightarrow L(β) (39%)
465.1061	0.0085	H-7(β) \rightarrow L(β) (28%), H-3(β) \rightarrow L(β) (31%).
366.0565	0.0191	H-6(β) \rightarrow L(β) (68%)
361.0044	0.0537	H-7(β) \rightarrow L(β) (30%),H-6(β) \rightarrow L(β) (17%), H-4(β) \rightarrow L(β) (15%)
358.4473	0.0028	H(α) \rightarrow L+3(α) (25%), H(β) \rightarrow L+4(β) (25%).
328.9817	0.0244	H-9(β) \rightarrow L(β) (37%), H-8 (β)L \rightarrow (β) (21%), H-7(β) \rightarrow L(β) (13%)
310.9222	0.0143	H-11(β) \rightarrow L(β) (35%), H-8(β)L \rightarrow (β) (37%)
307.0719	0.0036	H-1(α) \rightarrow L+6(α) (14%), H-11(β) \rightarrow L(β) (15%), H-1(β) \rightarrow L+7(β) (14%).

Table 9 .Calculated energies of the involved molecular orbitals in the electronic transitions and the percent distribution of these orbitals on Cu center, chloride ligand and organic ligand.

Spin	MO	Energy (eV)	Cu	Cl	Organic ligand
β	L+7	-0.44	5	0	95
β	L	-3.85	58	12	30
β	H	-6.43	0	0	99
β	H-1	-6.58	1	0	99
β	H-2	-7.2	3	86	11
β	H-3	-7.23	10	77	12
β	H-4	-7.69	21	39	40
β	H-5	-7.9	2	7	91
β	H-6	-8.05	1	3	96
β	H-7	-8.16	13	21	67
β	H-8	-8.52	4	2	94
β	H-9	-8.57	5	2	93
β	H-10	-8.67	7	1	92
α	L+6	-0.44	5	0	95
β	H-1	-6.59	1	1	99

The UV-Vis spectrum of complex **3** was calculated in water Figure **16**, there is good agreement between the calculated spectrum and the experimental one. There are three absorption bands in the calculated spectrum at 350 nm, 460 and 630nm.

The observed transitions are assigned as LMCT with the except of the shoulder at 307nm to LLCT, the population analysis of the electronic transitions indicates that all the main transitions occur from occupied molecular orbitals mainly on the ligands to LUMO- β molecular orbital, 58% of LUMO- β is located on the copper(II) center look at Table **9** and Figure **17**. When dien ligand was added to complex **3**, only one broad peak absorption maximum at 625nm was observed (blue).

The shift in $\lambda_{\text{max}} \cong 50\text{nm}$ for complex **3** after addition of dien ligand clearly confirmed the complete substitution of one dpa and Cl ligands with (dien) to form complex **4** look for that to Figure **15** as an illustrated in (Scheme **2**).

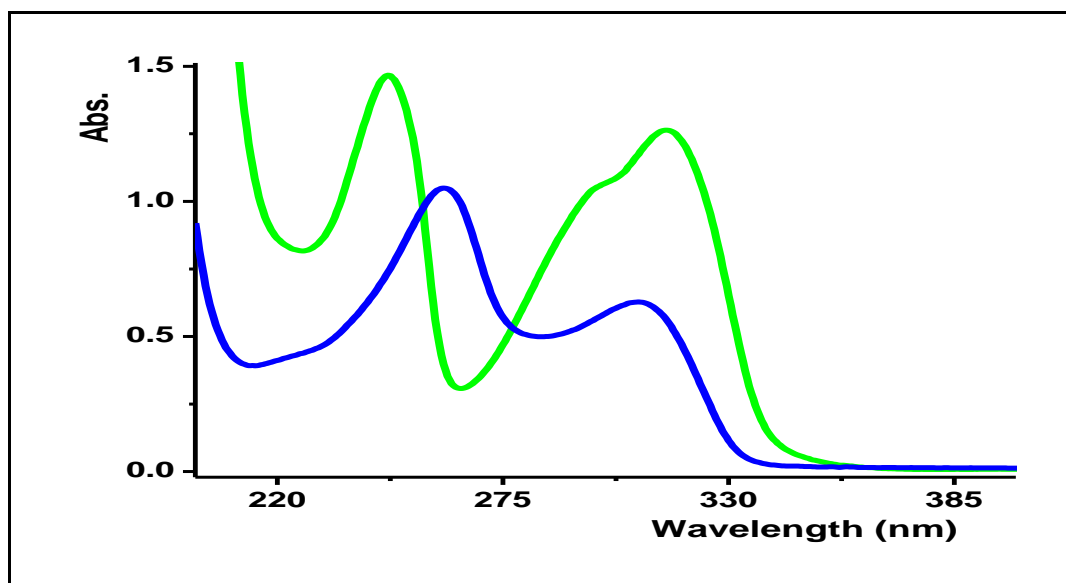


Figure 18. UV- spectra of $[\text{Cu Cl (2,2'-dpa)}_2]\text{Cl}$ green spectra and $[\text{Cu(2,2'-dpa)(dien)}]\text{Cl}_2$ blue spectra dissolved in water at (RT).

In the UV- region complex **3** exhibits two sharp peaks at $\sim 240\text{ nm}$ and 320 nm while complex **4** showed two singles at $\sim 245\text{ nm}$ and 310 nm , all were assigned to intra-ligand π to π^* electron transfer as in Figure **18**.

6. Crystal structure for complex **3**.

Complex **3** crystallizes in the Monoclinic $C12/c1$ space group. The crystal data and structure refinement parameters are given in Table **2** and selected bond distances and bond angles are given in Table **10** and Table **11**. The ORTEP diagram of the molecule with the atomic numbering and crystal packing are shown in Figure **19** and Figure **20**, respectively.

Table 10. measured bond length (Å) for Complex 3 crystal .

<u>Main bond between center copper ion and bonded nitrogen .</u>	<u>Bond lengths (Å)</u>
Cu(1)-N(8)	1.999(2)
Cu(1)-N(21)	2.019(2)
Cu(1)-N(1)	2.053(2)
Cu(1)-N(14)	2.157(2)
Cu(1)-Cl(1)	2.2987(8)

Table 11. Bond angle (N-Cu-N) for complex 3 crystal.

<u>Bond angle formed between copper surrounded by nitrogen ligand.</u>	<u>Bond angle [°]:</u>
N(8)-Cu(1)-N(21)	174.25(9)
N(8)-Cu(1)-N(1)	86.92(9)
N(21)-Cu(1)-N(1)	93.58(9)
N(8)-Cu(1)-N(14)	99.20(9)
N(21)-Cu(1)-N(14)	86.31(8)
N(1)-Cu(1)-N(14)	101.84(9)
N(8)-Cu(1)-Cl(1)	90.17(7)
N(21)-Cu(1)-Cl(1)	86.59(7)
N(1)-Cu(1)-Cl(1)	150.64(7)
N(14)-Cu(1)-Cl(1)	107.47(7)

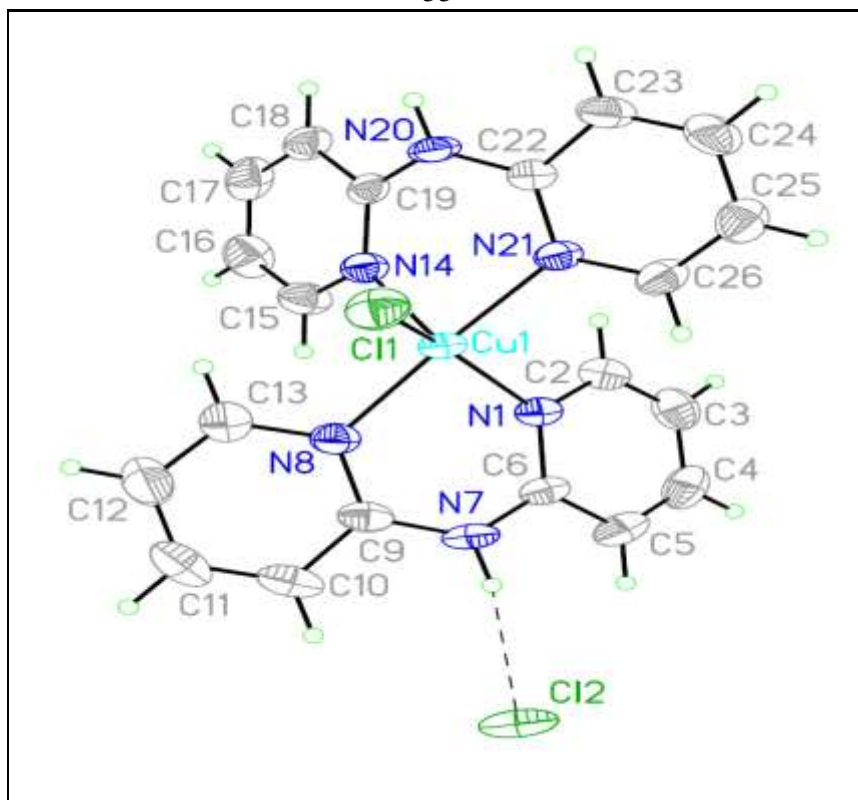


Figure 19. The ORTEP generated diagram of complex **3** with displacement ellipsoids drawn at 30% probability level, Hydrogen atoms are omitted for clarity.

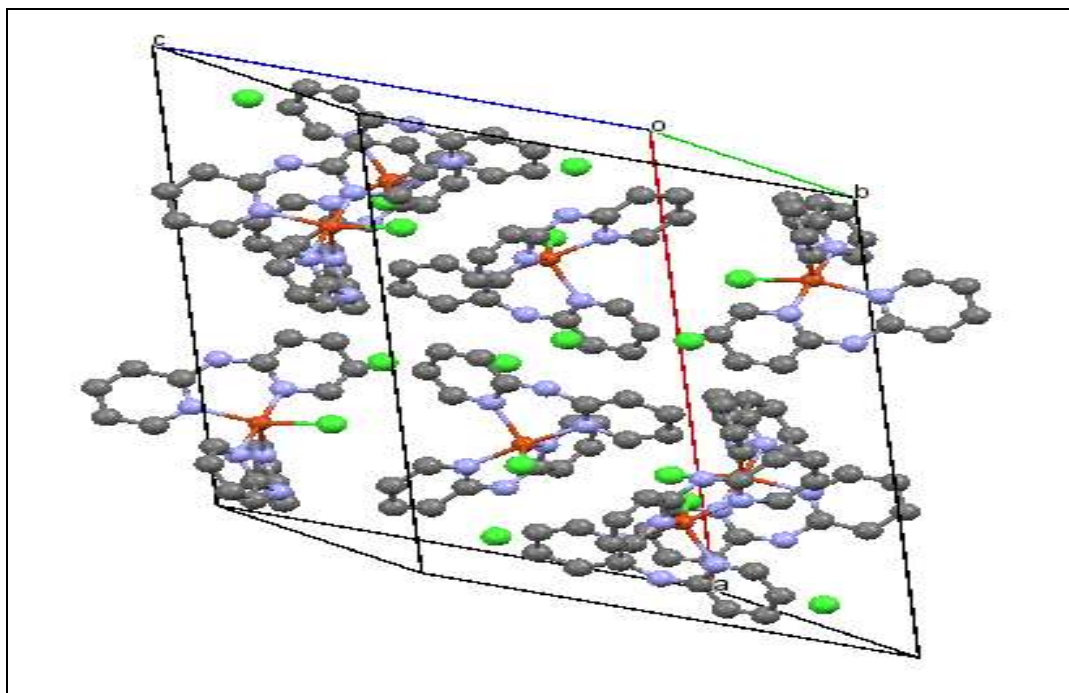


Figure 20. The crystal packing of the complex **3**.

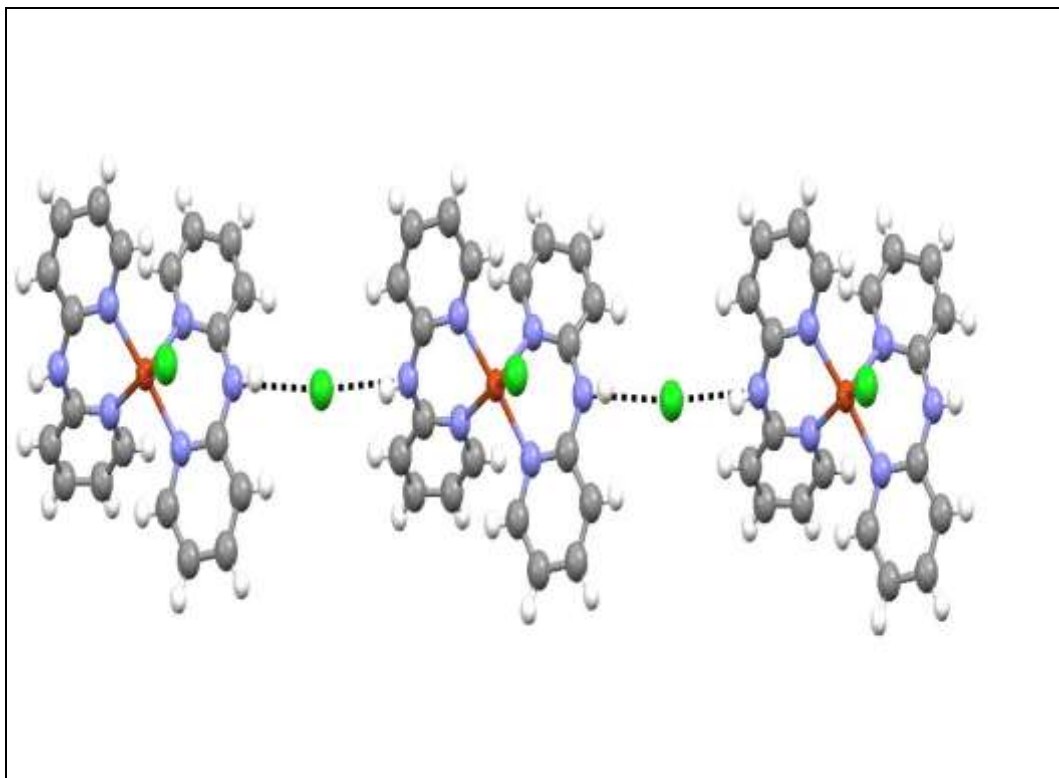


Figure 21. Chain structure of the complex **3**.

Cu(II) is four coordinated to the N atoms from two dpa ligands and one Cl ion. The acidic amine protons of both dpa ligands did not coordinate the Cu(II) center but stabilized the crystal structure through several intermolecular H-bonds as seen in Figure **21**, and the N-H didn't protonate upon complexation to the copper center to form tridentate ligand donor.

The four N atoms of dipyriddyamine ligand together with one Chloride ion coordinate the copper center with distorted square pyramidal geometry configuration with Cu(1)-N(1)= 2.053(2), Cu(1)-N(8)= 1.999(2), Cu(1)-N(21)= 2.019(2), Cu(1)-N(14)= 2.157(2) and Cu(1)-Cl(1)= 2.2987(8) Å.

7. Hirshfeld surface analysis of complex 3.

Hirshfeld surface analysis is an effective tool for exploring packing modes and intermolecular interactions in molecular crystals [86-88]. They

offer a visual picture of intermolecular interactions and of molecular shape in a crystalline environment. Surface features characteristic of different types of intermolecular interactions can be identified, and these features can be revealed by color coding distances from the surface to the nearest atom exterior (de plots) or interior (di plots) to the surface. In the crystal structure of complex **3** it mainly contain one H-bond N-H...Cl with 2.72Å Figure **22**, such interactions were confirmed by Hirschfield surface analysis as seen in Figure **23**.

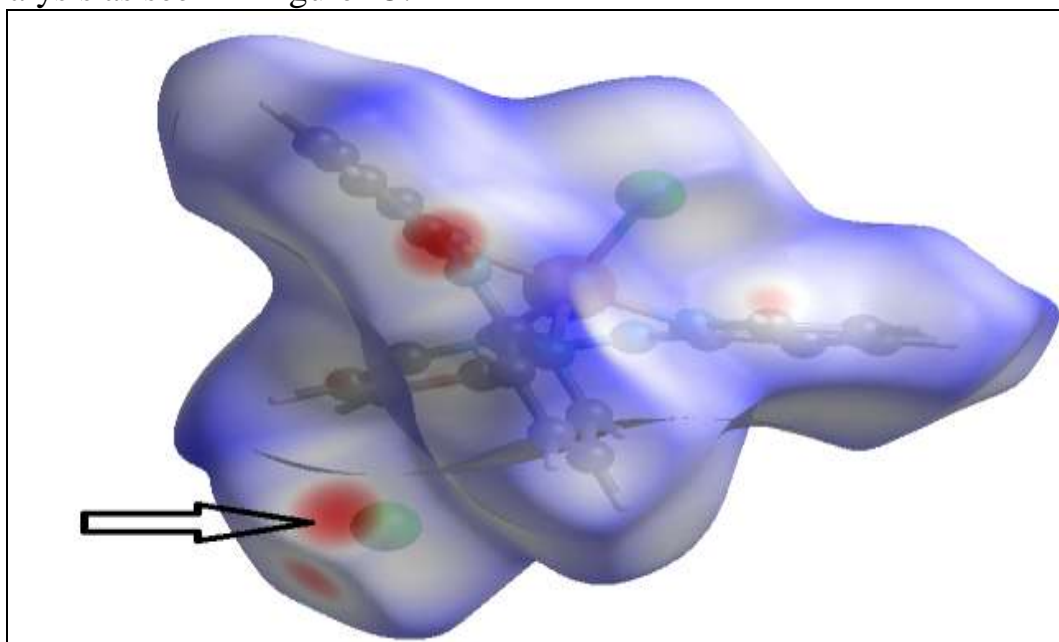


Figure 22. Hirschfield surfaces comprising *d_{norm}* surface plots for complex **3**.

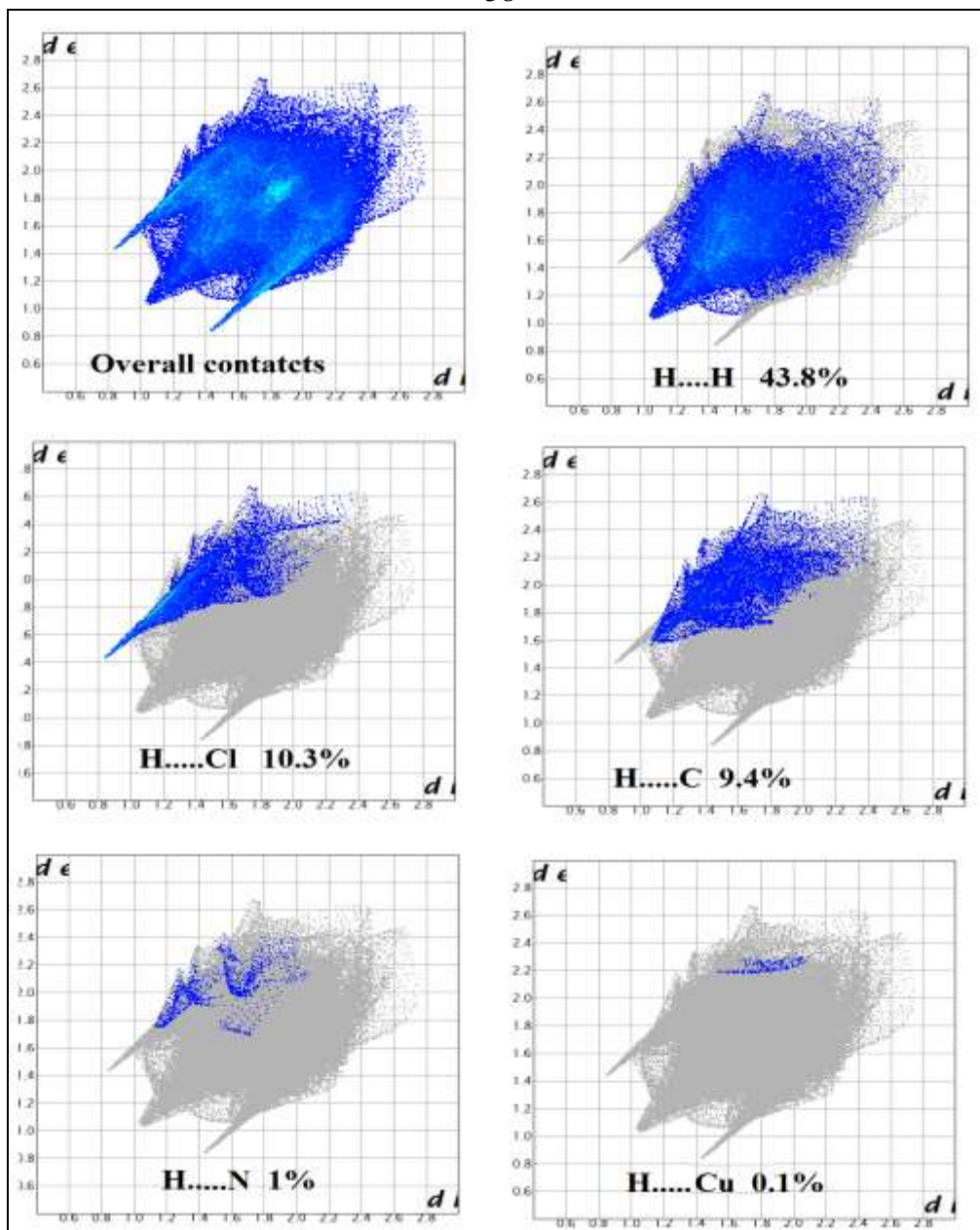


Figure 23. Fingerprint plots of the complex 3 molecule.

Hirschfeld surface analysis of the complex 3 proclaims that the dark spots occur on the surface as a result of hydrogen bond acceptors near the chloride which clearly stabilized such packing. The fingerprint plot for different atom...atom contacts in the complex 3 and the percentage of contribution of each contact to the Hirschfeld surface were illustrated in Figure 23.

PART3: Biological Studies and activity of complex 1 and 2.

1. Antioxidant activity (β -Carotene assay).

Three compounds were tested for their antioxidant activity using β -carotene model. Figure 24 shows the changes in values of absorbance with time for compounds (CuBr₂(phen), 1, and 2).

Complex 2 showed promising antioxidant activity (%AA= 47.1) compared with BHA (%AA= 77.2) and complex 1 (%AA= 35.8) figure25 show the %AA complexes.

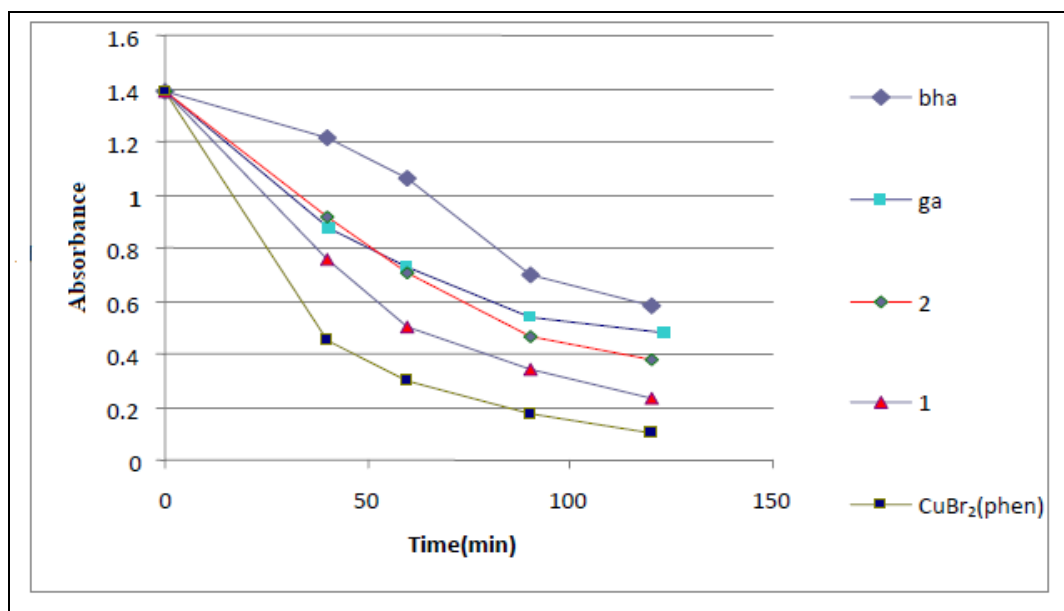


Figure 24. Changes in values of absorbance with time for starting compounds and products, BHA and Gallic acid as assessed by β -carotene-linoleic acid assay over 120 min.

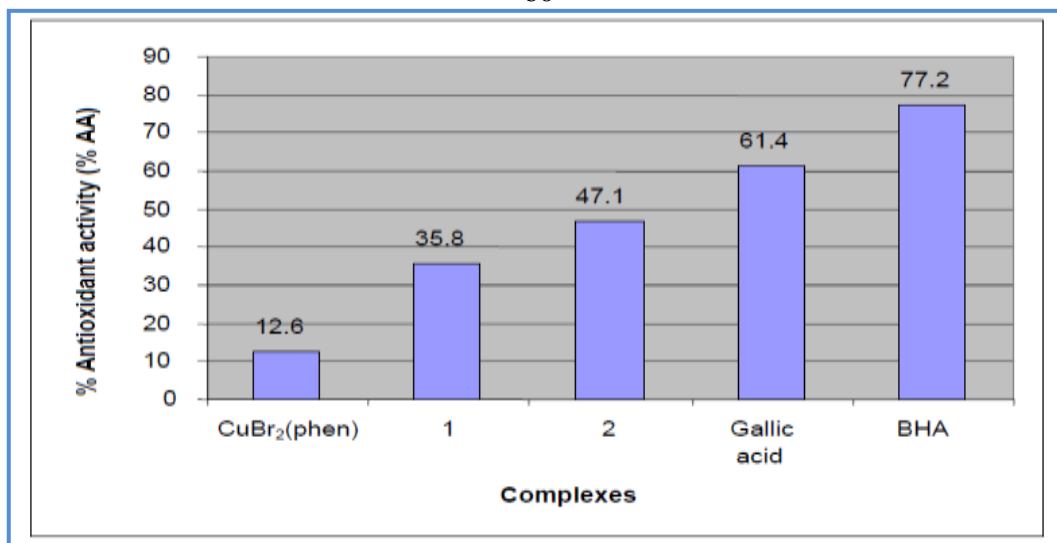


Figure 25. Antioxidant activities of methanol solution of the three copper compounds, and BHA and Gallic acid as assessed by β -carotene -linoleic acid assay over 120 min. The two complexes (**1** and **2**) showed higher activity compared to starting material CuBr₂(phen), which means that binding replacing the two bromide ligand with triamine ligands improved the ability of those complexes to react with the oxidants and delay bleaching color of β -carotene.

2. Antibacterial and anti-Candida activity.

The fundamental role of copper and the recognition of its complexes as important bioactive compounds *in vitro* and *in vivo* aroused an ever-increasing interest in these agents as potential drugs for therapeutic intervention in various diseases [76]. Complex **1** showed the highest activity against all tested bacteria with inhibition zone ranging (17.0 mm) against *S.typhi* to (11.5mm) against *E.coli*. The same compound also showed the highest anti-Candidal activity (20.4 mm). The activity was found to be in the range (43-70%) comparing to the reference antibiotic (gentamicin), and (66%) of amphotericin-B Complex **2** exhibited weak

activity against all bacteria and *Candida* isolates with inhibition zone diameter ranging from (8.5mm) against *E. coli* to (12mm) against *K. pneumonia* compared with complex **1** see Table 12

Table 12. Inhibition zone in (mm), each sample was done in triplicate.

Compounds	<i>Microbial strain tests.</i>						
	<i>P. vulgaris</i>	<i>S. aureus</i>	<i>E. coli</i>	<i>Aeruginosa</i> <i>Ps.</i>	<i>Sal. typhi</i>	<i>K. pneumonia</i>	<i>C. albicans</i> (5strains)
CuBr₂ (phen)	12.0±3.0*	14.0±0.0	14.0±0.0	13.0±1.0	12.75±1.25	15.0±0.0	12.6±2.3
1	13.0±0.50	13.75±0.2	11.5±0.5	14.5±2.5	17.0±0.0	14.5±1.50	20.4±2.4
2	10.0±0.0	10.5±0.50	8.5±0.50	10.0±0.0	10.0±0.0	12.0±0.0	6.1±5.6
Reference antibiotic* *	29.0±0.0	28.0±3.0	27.0±2.0	25+1.0	24.4±0.5	27.5±0.5	31.2±1.3

*Average values of inhibition zone diameter in mm ± SD. ** Gentamicin for bacteria, amphotericin for *C. albicans*.

The high broad spectrum activity for complex **1** could be mediated by targeting essential steps in microbial growth or by causing metabolic toxicity [52]. Our results are consistent with the previous findings that reported a broad antimicrobial activity of copper complexes against an array of pathogens [76].

3. Antifungal Activity.

The antidermatophytic activity of Complexes (CuBr₂(phen), **1**, and **2**) was tested against *M. canis* and *T. rubrum*. Figure 26 shows that the percent mycelial inhibition for the tested compounds (at 300 µg/mL) against the two dermatophytes.

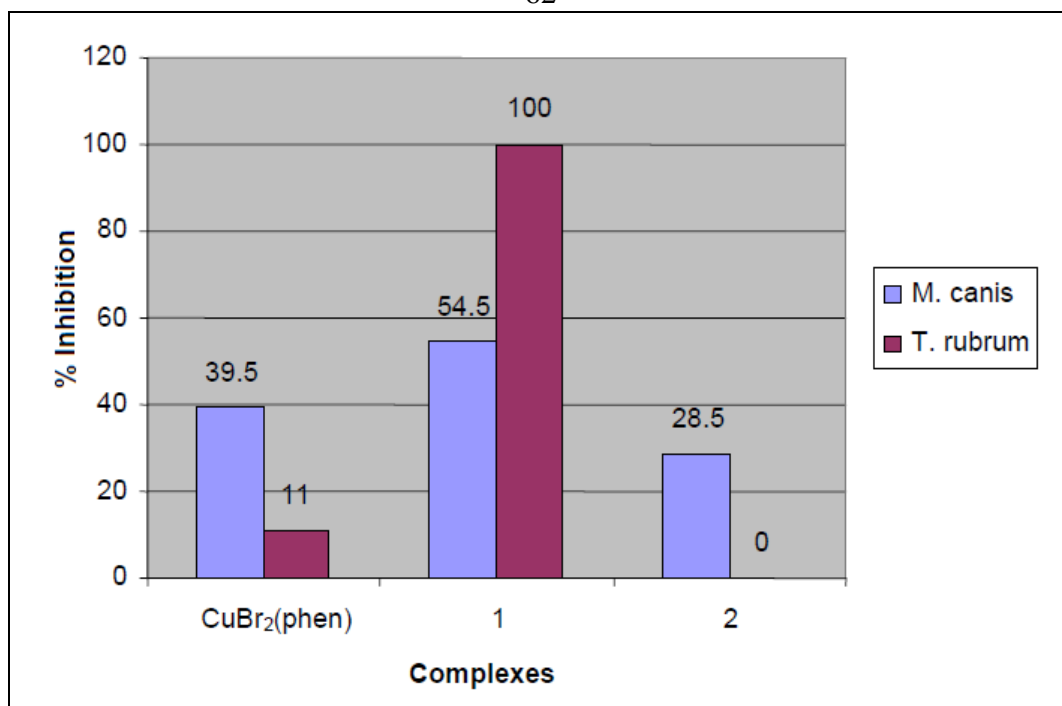


Figure 26. Anti-dermatophytes activity of CuBr₂(phen), **1** and **2** complexes (% inhibition) at 300 µg/mL.

Complex **1** revealed complete inhibition against the two types of dermatophytes. Also it showed a remarkable activity ranged from (50-100 %), compared to complex **2** and CuBr₂(phen). In this context, compound CuBr₂(phen) exhibited promising antifungal activity against all the tested fungi with MIC less than 100 µg/mL.

From our results we can suggest that compounds investigated in this study could find practical application in the introduction of highly active and safe antimycotics in addition to the limited commercial antifungal drugs.

4. Cytotoxicity determination of compounds on HCT116 Cells.

Colon cancer cells, HCT116, were exposed to the Complexes (CuBr₂(phen), **1**, and **2**) for 24h. No sign of toxicity observed for

complexes **1**, **2** and CuBr₂(phen) up to 200, 160, and 80 μM respectively in Figure 27.

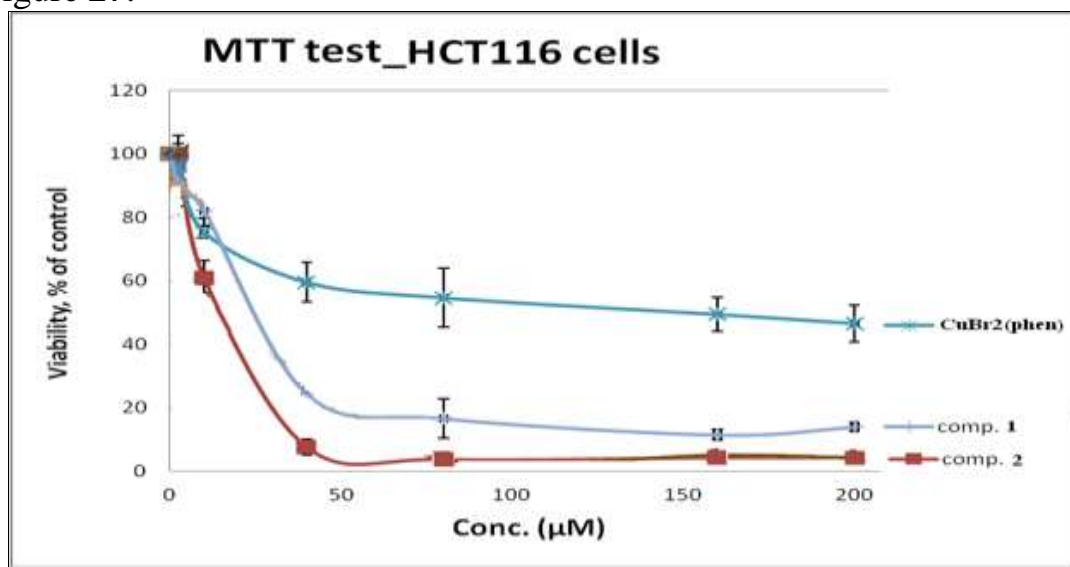


Figure 27. MTT assay in HCT-116 colon cancer cells after an overnight treatment with various concentrations of the complexes **1** and **2**.

However, the LD₅₀ for the compounds **2**, **1** and CuBr₂(phen) was around 20, 30 and 160 μM respectively. The toxicity order of the compounds tested from the most toxic complex to the lower toxicity: complex 2 > complex 1 > CuBr₂(phen).

5. DNA binding properties of complex 1.

The application of electronic absorption spectroscopy is one of the most useful techniques for DNA binding studies [77-82].

Complex binding with DNA through intercalation usually results in hypochromism and bathochromism, due to the intercalative mode involving a strong stacking interaction between an aromatic chromophore and the DNA base pairs. The extent of the hypochromism commonly parallels the intercalative binding strength.

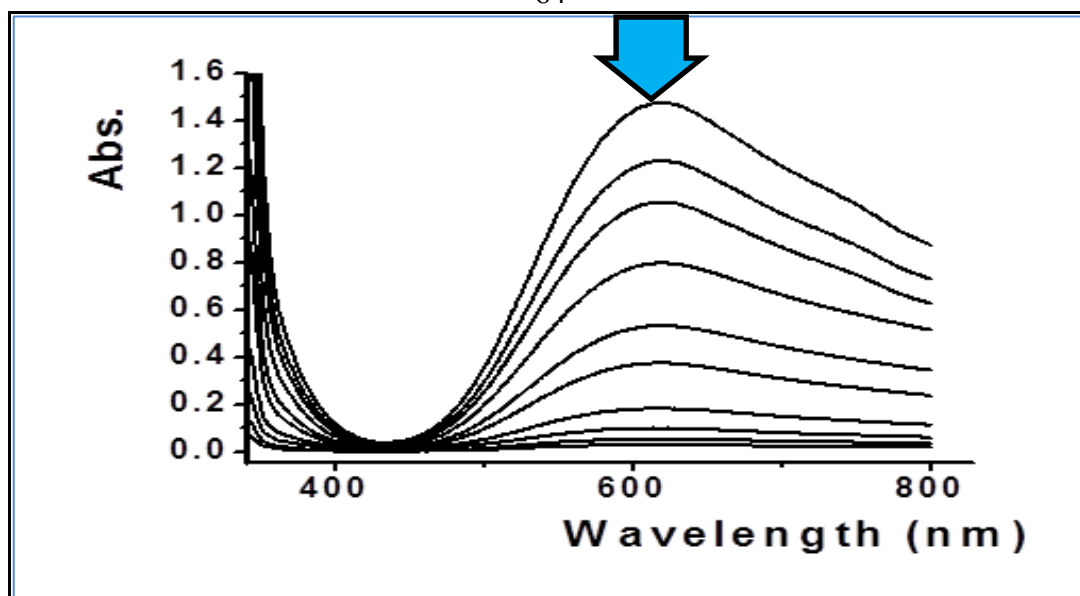


Figure 28. Electronic spectral titration of complex **1** with CT-DNA at 620 nm in Tris-HCl buffer; [complex]= 5×10^{-3} ; [DNA]: a= 0.0, b= 1.0×10^{-4} , c = 4.0×10^{-4} , d= 8.0×10^{-4} , e = 1.0×10^{-3} , f = 3.0×10^{-3} , h = 6.0×10^{-3} , i = 1.0×10^{-2} , j= 2.0×10^{-2} , k = 4.0×10^{-2} M. The arrow denotes the gradual decrease of the complex concentration upon DNA addition.

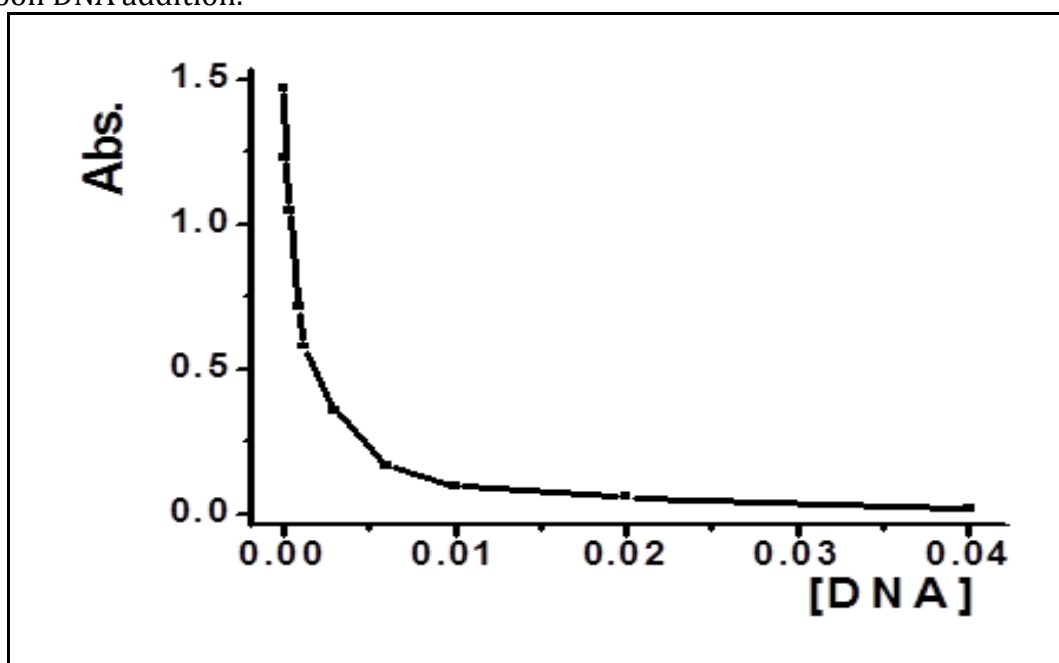


Figure 29. Absorption plot against [DNA] to confirm the exponential decreasing relation at $\lambda = 620$ nm.

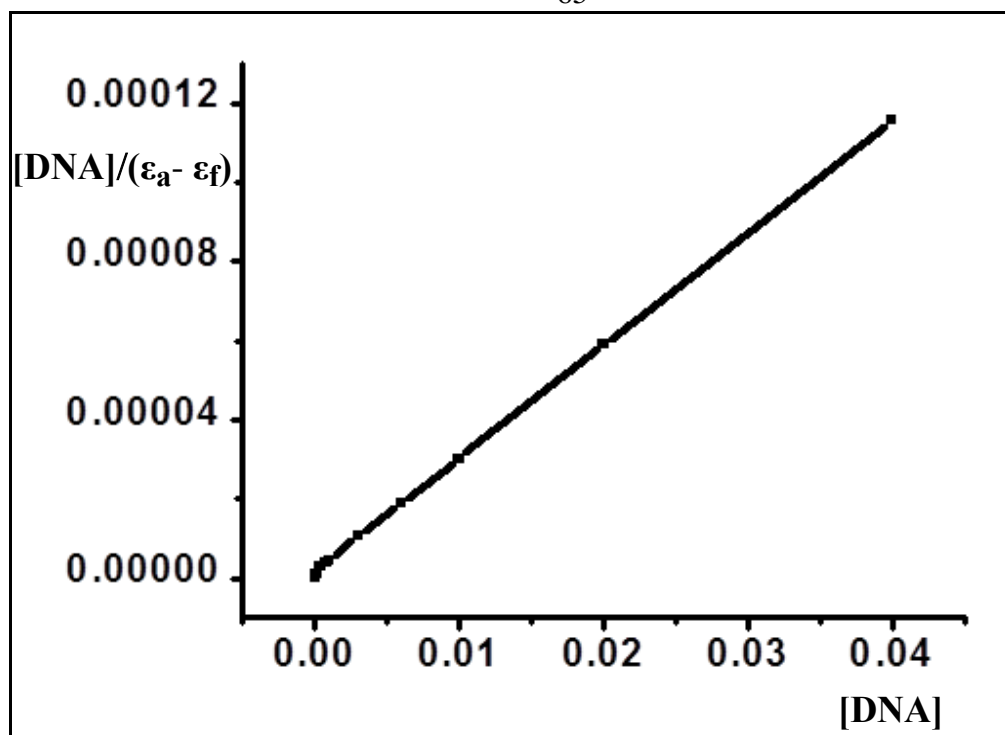


Figure 30. Plot of $[\text{DNA}]/(\epsilon_a - \epsilon_f)$ versus $[\text{DNA}]$ for the absorption titration of DNA with the complex **1**.

The electronic absorption spectrum of complex **1** in $5 \times 10^{-3} \text{M}$ Tris-HCl buffer exhibits bands around 620 and 280 nm. The band at 620 nm was used for the absorption spectral titration with CT-DNA. On incremental addition of $[0.0001-0.04] \text{M}$ DNA, the band shows sufficient decrease in absorption accompanied Figure **28** and Figure **29**.

In order to compare quantitatively the binding strength of complex **1**, the calculated intrinsic binding constant K_b was obtained by monitoring the changes in absorbance with increasing concentration of DNA using the following equation [77]:

$$[\text{DNA}]/(\epsilon_a - \epsilon_f) = [\text{DNA}]/(\epsilon_b - \epsilon_f) + 1/(K_b(\epsilon_b - \epsilon_f)).$$

Where in $[\text{DNA}]$ is the concentration of DNA in base pairs, ϵ_a , ϵ_f , and ϵ_b are the apparent, free and bound-metal-complex extinction coefficients

respectively, K_b is the equilibrium binding constant (in M^{-1}) of complex binding to DNA. When plotting $[\text{DNA}]/(\epsilon_a - \epsilon_f)$ vs $[\text{DNA}]$, K_b is obtained by the ratio of the slope to the intercept.

The binding constant K_b for complex **1** is found to be $8.6 \times 10^4 M^{-1}$ Figure **30**, These features are equivalent to those observed for Cu(II) complexes [76-83]. The results suggest an association of the compound with DNA and it is also likely that this complex binds to the helix by intercalation [79-83].

Chapter Four

Conclusion

Conclusion:

In part one two novel dicationic mixed amine-ligand of Cu(II) 1,10-phenanthroline / (dien) and (dipn) complexes were synthesized in high yields, and general formula complex **1** [Cu(Phen)(dien)]Br₂ and complex **2** [Cu(Phen)(dipn)]Br₂, displacement of bromide in CuBr₂(phen) by (dien or dipn) N-tridentate ligands from internal coordination sphere to the outer sphere was monitored by [IR and UV- visible spectra, MS-Spectrometry]. Single crystal X-ray diffraction for complex **1** showed that copper atom is coordinated with amines ligands as bromide salt is distorted trigonal bipyramidal geometry with *R* factor takes a value of **0.69**. The absorption spectrum of representative complex in water was modeled by time-dependent density functional theory (TD-DFT). The Self Assembly indicated that the N(π)...N interactions play significant role in stabilizing the final three-dimensional structure.

In part two Copper(II)chloride was treated with 2,2'-dipyridylamine ligand in methanol solvent, monocationic complex **3** [Cu(dpa)₂Cl]Cl was formed with high yield,

and single crystals X-Ray diffraction solved the square pyramidal geometrical structure of copper(II) coordinate with two dipyridylamine and one chloride ion and the other chloride that counter ion of complex.

Complex **3** was treated with equivalent moles diethylenetriamine ligand that empowered the high yield of complex **4** [Cu(dpa)(dien)]Cl₂ formation, the reaction was detected by color changes from green to blue, and monitored by physical measurement[UV-visible spectrum, IR-spectrum,

Melting point, MS-Spectra]. All measurement that proved the one dipyriddyamine ligand and coordinated chloride ion substituted by 3N-tridentate (dien) ligand.

In part three from biological studies for complex **1** and **2** antimicrobial and antiproliferative studies revealed that complex **1** and **2** has a remarkable antimicrobial activity against bacteria, Candida, and dermatophytes. Complex **1** exhibit strong DNA binding with binding constant ($K_b = 8.6 \times 10^4 \text{ M}^{-1}$) through absorption spectral titration. Also, both complexes **1**, **2** have shown high in vitro cytotoxic activity against cancer cells, as well as high antioxidant activity.

References

1. A. Cassol, P. Di Bernardo, R. Portanova, M. Tolazzi, G. Tomat, P. Zanonato, **J. Chem. Soc. Dalton Trans.** (1992) 469-474.
2. A. Dikshit, A. Husain, **J. Chem. Fito, terapia** 3 (1984) 171-176.
3. A.W. Addison, T. Nageswara-Rao, J. Reedijk, J. van Rijn, G.C. Verschoor, **J. Chem. Soc. Dalton Trans.** (1984) 1349-1356.
4. Agilent Technologies, **J. Crys, Alis. Pro**, 16 (2011) 171
5. Awwadi, F. F.; Willett, R. D.; Peterson, K.; Twamley, **B. J. Phys. Chem.** 111 (2007) 2319-2328.
6. B. Kurzak, K. Bogusz, D. Kroczevska, **J. Jezierska, Polyhedron.** 20 (2001) 2627-2636.
7. B.H. Yun, J.O. Kim, B.W. Lee, P. Lincoln, B. Nordén, J.-M. Kim, S. K. Kim, **J. Phys. Chem.** 107 (2003) 9858-9864.
8. B.Q. Ma, S. Gao, T. Yi, **C.H. Yan, Inorg. Chem Com.** 3 (2000) 93-95.
9. B.W. Lee, S.J. Moon, M.R. Youn, J.H. Kim, H.G. Jang, S.K. Kim, **J. Bio. phys.** 85 (2003) 3865-3871.
10. C. Janiak, Dalton Transactions, **J. Chem, Soci.** 14(2003) 2781-2804.
11. C. Lee, W. Yang, R.G. Parr, **J. Phys. Rev.** 37 (1988) 785-789.
12. C. M. Liu, R. G. Xiong, **J. Liq, Polyhedron.** 15 (1996) 4565-4571.
13. C. Tsiamis, M. Themeli, **J. Inorg. Chim. Acta** 206 (1993) 105-115.
14. D. Chatterjee, A. Mitra, R.E. Shepherd, **Inorg, Chem. Acta.** 357 (2004) 980-990.
15. E. Jawetz, J.L. Melnick, E.A. Adelberg, G.F. Brooks, J.S. Batel, L.N. Ornston, **J. Medi. Micro. Biol.** 20 (1995) 21-26.

16. E.C. O'Brien, E. Farkas, M.J. Gil, D. Fitzgerald, A. Castineras, K.B. Nolan, **J. Inorg. Bio chem.** 79 (2000) 47-51.
17. E.M. Boon, J.K. Barton, **Curr. Opin. Struct. Biol.** 12 (2002) 320-329.
18. F. Awwadi, F; Willett, R. D; Twamley, **J. Chim. Cryst. Growth Des.** 7 (2007) 624-632.
19. F. Gandara; Fortes-Revilla, C; Snejko, N; Guti_errezz-Puebla, E; Iglesias, M; Monge, M. A. **Inorg. Chem.** 45(2006) 9680-968
20. F. Westerlund, P. Nordall, J. Blechinger, T.M. Santos, B. Nordén, **J. Phys. Chem.** 112 (2008) 6688-6694.
21. F.A. Cotton, B. Hong, Prog, **Inorg. Chem.** 40 (1992) 179–289.
22. G. M., Ed.;Bruker AXS Inc, Madison, WI, SHELXTL, Sheldrick, **Strc. Determ. Soft, Suite.** (2001) 6-10
23. G. Murphy, P. Nagle, B. Murphy, B. Hathaway, **J. Chem. Soc. Dalton Trans.** (1997) 2645-2652.
24. G.A. Gazzani, A. Papetti, G. Massolini, M. Daglia. **J. Agric. Food Chem.** 46 (1998) 4118- 4122.
25. GA Gazzani, Papetti GM, Daglia M. **J. Agric. Food Chem.** 46 (1998) 411-822.
26. H. Chowdhury, R. Ghosh, S.H. Rahaman, G.M. Rosair, B.K. Ghosh, **Ind. J. Chem.** 44 (2005) 687.
27. I. Wiegand, K. Hilpert, R.E. W. Hancock, **Natu. Protocols.** 3 (2008) 163-175.
28. J. Szklarzewicz, A. Samotus, J. Burgess, J. Fawcett and D. R. Russell, **J. Chem. Soci.**18 (1995) 3057- 3061.

29. J.A. Cowan, **Chem. nucleases, Chem. Biol.** 5 (2001) 634-642.
30. J.C. Hierso, R. Amardeil, E. Bentabet, R. Boussier, B. Gautheron, P. Meunier, P. Kalck, **Coord. Chem. Rev.** 236 (2003) 143-206.
31. J.K. Hurst, **Coord. Chem. Rev.** 249 (2005) 313–328.
32. J.L. García-Giménez, M. González-Álvarez, M. Liu-González, B. Macías, J. Borrás, G. Alzuet, **J. Inorg. Biol. chem.** 103 (2009) 923-934.
33. J.M. Kim, K.-M. Lee, J.Y. Choi, H.M. Lee, S.K. Kim, **J. Inorg. Biochem.** 101 (2007) 1386-1393.
34. J.R. Morrow, O. Iranzo, **Syn. Meta. nucleases, Curr. Opin. Chem. Biol.** 8 (2004) 192-200.
35. J.Y. Choi, J.-M. Lee, H. Lee, M.J. Jung, S.K. Kim, J.M. Kim, **Bio. phys. Chem.** 134 (2008) 56-63.
36. K. Nagaraj, S. Ambika, Sh. Rajasri, S. Sakthinathan, S. Arunachalam, **Colloids and Surfaces** .122 (2014) 151-157.
37. K. Nakamoto, **Inorg. Coord. Comp, 4th ed. J. Wiley & Sons: NY,**(1986) 140-184.
38. K. S. Saikat, **J. Mol. Struc.** 70 (2014) 1064.
39. K. Takamiya, **J. Nat, chem** (1960) 185-190.
40. L. Nad, A. Agents, **Clin. Micro, Biol. Infection.** 6 (2000) 509-515.
41. L.J.K. Boerner, J.M. Zaleski, **Curr. Opin. Chem. Biol.** 9 (2005) 135-144.
42. M. A. Spackman, J. J. McKinnon, **Crys. Eng. Comm.** 4 (2002) 378
43. M. A. Spackman, J. J. McKinnon, D. Jayatilaka, **Cryst. Eng. Comm.** 10 (2008) 377.

44. M. Al-Noaimi, M. I. Choudhar, F. F. Awwadi, W. H. Talib, T. Ben Hadda, S. Yousuf, A. Sawafta, I. Warad, **J. Spect. Molec. Biomolec Chim. Acta.** 127 (2014) 225-230.
45. M. Cossi, N. Rega, G. Scalmani, V. Barone, **J. Comput. Chem. Draw.** 24 (2003) 669-681.
46. M. Gonzalez-Alvarez, A. Pascual-Alvarez, L.D. Agudo, A. Castineiras, M. Liu-Gonzalez, **J. Borrás, Dalton. Trans.** 42 (2013) 10244-10259.
47. M.E. Núñez, J.K. Barton, **Curr. Opin. Chem. Biol.** 4 (2000) 199-206.
48. M.J. Chare, P.C. Hydes, **J. Metal Ion in Bio Sys.** 2 (1980) 1-62.
49. M.J. Frisch, G.W. Trucks, H.B. Schlegel, G.E. Scuseria, V. Bakken, C. Adamo, J. Jaramillo, R. Gomperts, J.B. Foresman, **J. Fox, Gaussian Inc, Wallingford CT, Gauss View, Gaussian, Pittsburgh,** (2009) 509.
50. M.K. Casida, C. Jamorski, K.C. Casida, D.R. Salahub, **J. Chem. Phys.** 108 (1998) 4439-4449.
51. M.S. Al-Saikhan, Howard L.R., Miller **J. Food. Chem. Sci.** 60 (1995) 341-343.
52. M.S. Al-Saikhan, L.R. Howard, J.C. Miller, **J. Food Sci.** 60 (1995) 341-343
53. Murray, P.R., Baron, E.J., Pfaller, M.A., Tenover, F.C. and Tenover, R.H. **Man. Clin, Mic. Bio.** (1995) 24-28.
54. N.M. O'Boyle, A.L. Tenderholt, K.M. Langner, **J. Comput. Chem.** 29 (2008) 839-845

55. P. A. Vigato, S. Tamburini, **J.Cord, Chem. Rev.** 248 (2004) 1717-2128.
56. P. K. Bowyer, K. A. Porter, A. D. Rae, A. C. Willis and S. B. Wild, **J. Chem Soci, Chem.Com .** 10 (1998) 1153-1154.
57. P. Kopf-Maier, H. Kopf, **Chem , Rev.** 87 (1987) 1137-1152.
58. P. M .Wayne, **Nati. Com. Clin. Lab, Sta .** (2012) 27-30.
59. P. Nordall, F. Westerlund, L.M. Wilhelmsson, B. Nordén, P. Lincoln, **Angew. Chem. Inter.** 46(2007) 2203-2206.
60. P. Vijayan, P. Vijayaraj, P. Setty, C. Hariharpura, A. Godavarthi, S. Badami, D.Arumugam, S. Bhojraj, **J. Biol. Pharm, Bollu.** 24 (2004) 528-530.
61. P. Wayne, **Nati Com, Clinical Lab Standards.** (2012) 27.
62. P.J. Hay, W.R. Wadt, **J. Chem. Phys.** 82 (1985)270-283.
63. P.R .Murray, E.J. Baron, M.A. Pfaller, F.C. Tenover, R.H. Yolke, Washington .D,C , **J. Man, Clin, Microbiology.** (1995) 47-68.
64. R. Bauernschmitt, R. Ahlrichs, **Chem. Phys. Lett.** 256 (1996) 454-464.
65. R. Ziessel, **J. Cord, Chem. Rev.** 216 (2001) 195-223.
66. R.D. Hancock, L, **J. Bartolotti, Inorg. Chem.** 44 (2005) 7175-7183.
67. R.E. Stratmann, G.E. Scuseria, M.J. Frisch, **J. Chem. Phys.** 109 (1998) 8218-8224.
68. R.G. Pearson, **Inorg. Chim. Acta.** 240.(1995) 93-98.
69. R.J. Sorenson, **J. Chem. Bio chem.** 16 (1984) 1110-1113.
70. R.K. Gouch, T.W. Kensler, L.W. Oberley, **J. Bio chem and Inorg Copper Chem.** 1 (1986) 139-156.

71. R.N Patel., N Singh., K.K.Shukla, J.Niclós-Gutiérrez, A.Castineiras, V.G. Vaidyanathan, **B.Unni Nair Spect. Chim. Acta** 62 (2005) 261-268.
72. R.N. Patel, A.P. Patel, K.B. Pandeya, **Ind. J. Chem.** 38 (1999) 900-905.
73. R.N. Patel, H.C. Pandey, K.B. Pandeya, **Ind. J. Chem.** 36 (1997) 809-811.
74. R.N. Patel, K.B. Pandeya, **Trans. Met. Chem.** 24 (1999) 35-37.
75. R.N. Patel, N. Singh, R.P. Shrivastava, S. Kumar, K.B. Pandeya, **J. Molecular . Liq.** 49 (2000) 95-99.
76. R.N. Patela, Nripendra Singha, K.K. Shuklaa, J. Niclós-Gutiérrezb, A. astineirasb,1, V.G. Vaidyanathanc, **Spec. Chim. Acta. Part** 62 (2005) 261-268.
77. S. Destri, M. Pasini, W. Porzio, F. Rizzo, G. Dellepiane, M. Ottonelli, G. Musso, F. Meinardi, L. Veltri, **J. Lumin, chim.** 127 (2007) 601.
78. S. Destri, M. Pasini, W. Porzio, F. Rizzo, G. Dellepiane, M. Ottonelli, G. Musso, F. Meinardi, L. Veltri, **J. Lumin. Chem.** 127 (2007) 601-605.
79. S. Goubatsis, S.P. Perlepes, I.S. Butler, N. Hadjiliadis, **J. Polyhedron. Chem.**18 (1999) 2369-2375.
80. S. Tabassum, S. Amir, F. Arjmand, C. Pettinari, F. Marchetti, N. Masciocchi, G.Lupidi, R. Pettinari, Eur, **J. Med. Chem.** 60 (2013) 216-232.
81. S. Youngme, C. Chailuecha, G.A. van Albada, C. Pakawatchai, N. Chaichit, J. Reedijk, **Inorg. Chim. Acta.** 358(2005) 1068.

82. T. Fujiwara, Iwamoto, E; Yamamoto, Y. **Inorg. Chem.** 23(1984) 115-117.
83. V.M. Manikandamathavan, V. Rajapandian, A.J. Freddy, T. Weyhermuller, V. Subramanian, B.U. Nair, **J. Eur. Med. Chem.** 57 (2012) 449-458.
84. W.J. Song, Q.Y. Lin, W.J. Jiang, F.Y. Du, Q. Y. Wei, **Spect. Chim. Acta.** 137 (2014) 122-128.
85. WI, Sheldrick, G.M. SHELXTL Madison. **version Structure determination software suite. Bruker AXS Inc.** 6 (2000) 10
86. X.B. Fu, Z.H. Lin, H.F. Liu, X.Y. Le, **Spect. Chim. Acta** 122 (2014) 22-33.
87. Y.J. Jang, B.-H. Kwon, B.-H. Choi, C.H. Bae, M.S. Seo, W. Nam, S.K. Kim, **J. Inorg. Bio chem.** 102 (2008) 1885-1891.
88. Y.S. Mary, P. Jojo, C.Y. Panicker, C.V. Alsenoy, S. Ataei, I. Yildiz, **J. Spect. chim. Acta.** 122 (2014) 499-511.

جامعة النجاح الوطنية
كلية الدراسات العليا

تصميم وأطياف وتركيب بنائي معقدات النحاس الثنائي ثلاثية متصلات النيتروجين ودراسة أثرها البيولوجي

إعداد

مهيب رافع محمد فقها

إشراف

أ.د. إسماعيل وراذ

قدمت هذه الأطروحة استكمالاً لمتطلبات الحصول على درجة الماجستير في الكيمياء بكلية الدراسات العليا في جامعة النجاح الوطنية- نابلس- فلسطين.

2015

ب
تصميم واطياف وتركيب بنائي معقدات النحاس الثنائي ثلاثية متصلات النيتروجين ودراسة اثرها
البيولوجي .
إعداد
مهيب رافع محمد فقها
إشراف
أ.د. إسماعيل وراذ

الملخص

حيث لوحظت تغيرات لألوانها بينما كان يتم اضافة الامينات للارتباط مع ايون الفلز الموجب لتكون المركبات من اللون البني الى اللون الازرق الفاتح ثم اللون الغامق وايضا من اللون البني للون الاخضر ثم للون الازرق ، وجميع هذه التغيرات في اللون تم تأكيدها باستخدام جهاز الامتصاص Uv-visible spectroscopy وجهاز الأشعة تحت الحمراء Infra-red spectroscopy من خلال الأطوال الموجية والعدد الموجي، وجهاز مطياف الكتلة في معرفة الكتلة المولية الصحيحة (M/z) وجهاز التحليل الكتلي الحراري في معرفة تأثير ارتفاع درجات الحرارة على استقرار تلك المركبات الأربعة فوجد بأنها ثابتة عند درجات الحرارة العادية إلى أن تصل حوالي 100 درجة مئوية وأكثر .

ومن الناحية الحيوية تم دراسة تأثير المركبات 1 و 2 على عدة امراض مثل سرطان القولون والفطريات الجلدية والبكتيريا وغيرها، وحيث اثبت ان هذه المركبات لها قدرة عالية للقضاء على تلك الامراض، وأن لهذه المركبات فعالية عالية للاتحاد مع الحمض النووي CT-DNA (binding) حيث أن ثابت الارتباط مع DNA = $8.6 \times 10^4 M^{-1}$ ، كما تمت دراسة تأثير المركبين 1 و 2 والمادة الاولية [Cu(phen)(Br)₂] لخلية سرطانية من القولون، حيث ظهرت السمية العالية للمركب 2 في تدمير الخلايا السرطانية للقولون .

كيمياء المعقدات الفلزية لها دورا هاما في مجالات الصناعة، كمجالات الطب والصيدلة والحفازات الكيميائية. حيث تم العمل على تصنيع مركبات للعناصر الكيميائية الانتقالية كالنحاس والبلاتين وذلك لفعاليتها في القضاء على الأمراض مثل السرطان والفطريات الجلدية والبكتيريا، والأوبئة الفتاكة، و في هذا البحث تم تصنيع أربع مركبات حديثة لمعقدات النحاس الثنائي الموجب من خلال معالجة أملاح النحاس CuBr₂ و CuCl₂ مع الامينات ثنائية وثلاثية المنح، لينتج المركبات

الكيميائية المعقدة التالية: (1) $[\text{Cu}(\text{phen})(\text{dien})]\text{Br}_2$ و (2) $[\text{Cu}(\text{phen})(\text{dien})]\text{Br}_2$ ،
(3) $[\text{Cu}(\text{dpa})_2\text{Cl}]\text{Cl}$ ، (4) $[\text{Cu}(\text{dpa})(\text{dien})]\text{Cl}_2$.

أثبتت تكون هذه المركبات بالحصول على بلوراتها ودراستها باستخدام جهاز أشعة الحيويد- السينية (Single Crystal - XRD) والقياسات الفيزيائية والكيميائية مثل امتصاص أطيف الأشعة تحت الحمراء (IR-Spectrum) وامتصاص أطيف الأشعة فوق البنفسجية (UV-Spectrum) ودرجات الانصهار والتحليل الحراري الكتلتي (TGA/ DTA Thermo- Graphmetric) Analysis (جهاز مطيف الكتلة MS-Mass Spectroscopy) حيث أكدت هذه القياسات أن الأشكال الفراغية الهندسية هرم رباعي غير منتظم للمركب 1 وهرم رباعي غير منتظم أيضا للمركب 3 ، وقياس اطوال الروابط الكيميائية بين ذرة النحاس وذرات النيتروجين ، والزوايا الرئيسية المحيطة بالذرة المركزية الأساسية.